The rheology of the meibomian lipid layer in health and disease: determination of viscoelasticity of thin lipid layers using the Quartz Crystal Microbalance with Dissipation (QCM-D)

A dissertation submitted for the degree of:

Doctor in philosophy

By:

Silvia del Carmen Jonguitud Flores

Under the guidance of:

Bernardo Yáñez Soto

&

Juan Rodrigo Vélez Cordero

San Luis Potosi, S.L.P

February, 2025

INSTITUTO DE FÍSICA

POSGRADO EN CIENCIAS INTERDISCIPLINARIAS

La reología de la capa de lipidos meibomiales en la salud y la enfermedad: determinación de la viscoelasticidad de capas lipídicas finas mediante la microbalanza de cristal de cuarzo con disipación (QCM-D)

Tesis que para obtener el grado de:

Doctora en Ciencias Interdisciplinarias

Presenta:

Silvia del Carmen Jonguitud Flores

Línea de investigación:

Biofísica y Bioingeniería

Director de tesis:

Bernardo Yáñez Soto

Co-director:

Juan Rodrigo Vélez Cordero

San Luis Potosi, S.L.P

Febrero, 2025

INSTITUTO DE FÍSICA

POSGRADO EN CIENCIAS INTERDISCIPLINARIAS

Abstract

An essential component for vision is the eye surface, which is constituted by the lid margin, the cells that cover up the expose area of the eye, and the tear film. The tear film is a complex colloidal system, form by the mucin-gel layer, the aqueous layer and the lipid film on the outermost surface. The lipid film is composed mostly by meibomian gland lipids, Among its many functions it retards tear film evaporation. An increased evaporation rate is related to evaporative dry eye syndrome. Dry eye syndrome is one of the most common reasons for visits to the ophthalmologist. People who suffer from this disease see their quality of life affected due to the impairment of visual function and the aggravating symptoms it causes. The predominant cause of dry eye disease is meibomian gland dysfunction (MGD), in a healthy eye, meibum should be liquid-like at body temperature so that it can move through the tubes of the meibomian gland and out of the gland through its openings, to finally spread onto the surface of the tear film. When meibum lipids come into touch with the surface of the eye, they cool down, which makes them more rigid. In pathological conditions changes in meibum composition leads to variations in melting and spreading properties. The physical qualities of meibum may be essential for the operation of the tear film. Examining rheological qualities is essential, as they depend on the compressive and expansive forces generated by the movements of the eyeball or eyelid, together with the velocities and amplitudes of these movements. Limited research has been performed on the bulk rheology of human meibum. We propose the use of the Quartz crystal microbalance with dissipation (QMC-D), as it works by linking changes in the frequency of the a quartz gold coated sensor with changes in the amount of mass absorbed by its surface, additionally it monitors changes in energy loss, providing a valuable insight into the viscoelastic properties of the system under study. In this work, we successfully measured the rheology of individual meibomian lipid samples, whereas it is typical to assess mixed samples from multiple individuals. The clinical differentiation between healthy and pathological states, such as dry eye or meibomian gland dysfunction (MGD), has been constrained by the lack of objective evaluations. The QCM-D may serve as a

method to clarify the variations in viscous and elastic moduli with temperature in both healthy and sick conditions.

Resumen

Un componente esencial para la visión es la superficie ocular, que está constituida por el margen del párpado, las células que recubren la zona expuesta del ojo y la película lagrimal. La película lagrimal es un sistema coloidal complejo, formado por la capa de mucina-gel, la capa acuosa y la película lipídica en la superficie más externa. La película lipídica está compuesta principalmente por lípidos de las glándulas de Meibomio y, entre sus muchas funciones, se encuentra la de retardar la evaporación de la película lagrimal. Un aumento de la tasa de evaporación está relacionado con el síndrome del ojo seco evaporativo. El síndrome del ojo seco es uno de los motivos más frecuentes de visita al oftalmólogo. Las personas que padecen esta enfermedad ven afectada su calidad de vida debido al deterioro de la función visual y a los síntomas agravantes que provoca. La causa predominante de la enfermedad del ojo seco es la disfunción de la glándula de Meibomio (DGM). En un ojo sano, el meibum debe ser líquido a temperatura corporal para que pueda desplazarse por los conductos de la glándula de Meibomio y salir de la glándula a través de sus orificios, para finalmente extenderse por la superficie de la película lagrimal. Cuando los lípidos del meibum entran en contacto con la superficie del ojo, se enfrían, lo que los hace más rígidos. En condiciones patológicas, los cambios en la composición del meibum provocan variaciones en las propiedades de fusión y extensión. Las cualidades físicas del meibum pueden ser esenciales para el funcionamiento de la película lagrimal. Examinar las propiedades reológicas es esencial, ya que dependen de las fuerzas de compresión y expansión generadas por los movimientos del globo ocular o del párpado, junto con las velocidades y amplitudes de estos movimientos. Se han realizado pocas investigaciones sobre la reología del meibum humano. Proponemos el uso de la microbalanza de cristal de cuarzo con disipación (QMC-D), ya que funciona vinculando los cambios en la frecuencia de un sensor de cuarzo recubierto de oro con los cambios en la cantidad de masa absorbida por su superficie, además monitoriza los cambios en la pérdida de energía, proporcionando una valiosa visión de las propiedades viscoelásticas del sistema en estudio. En este trabajo, medimos con éxito la reología de muestras

individuales de lípidos meibomianos, mientras que es típico evaluar muestras mixtas de múltiples individuos. La diferenciación clínica entre estados sanos y patológicos, como el ojo seco o la disfunción de las glándulas de Meibomio, se ha visto limitada por la falta de evaluaciones objetivas. La QCM-D puede servir como método para aclarar las variaciones de los módulos viscoso y elástico con la temperatura tanto en estados sanos como patológicos.

Index

Figure index

1. Introduction

The outermost part of the tear film is the tear film lipid layer (TFLL) mostly composed of a complex mixture of various polar and nonpolar lipids, this secretions (meibum) spread over the ocular surface as an ideally continuous film over the mucoaqueous layer of the tear film, forming a duplex film with an estimated thickness around 15-160 nm, according to the most accepted view on the structure of the TFLL, the polar lipids lay down above the mucoaqueous layer as a thin film with a relatively thick layer of nonpolar lipids below it[1,3,5-8]. Formed structure helps resist the collapse of tear film on the ocular surface, facilitates the formation of a thin tear film, and slows tear film evaporation[9-11]. An increased evaporation rate is related to evaporative dry eye syndrome. Dry eye syndrome has a great impact on visual function of people suffering it from, affecting its quality of life, due to symptoms like: burning or feeling of pressure in the eyes, sensation of sand or foreign body, tearing, pain that may be localized somewhere in the eye, behind the eye or even around the orbit; redness is a common complaint, intermittent blurred vision that may also be described as halos around lights at night, feeling of heaviness in the eyelids or difficulty opening the eyes, dryness and tired eyes[12-13]. The predominant cause of this type of dry eye disease is meibomian gland dysfunction (MGD), possibly due to changes in meibum composition leading to variations in melting and spreading properties of meibum. One of the conventional treatments for MGD is warming the eyelids at a temperature above the melting point of meibum, since variations in the melting point of meibum from MGD sufferers occurs, by being composed of a complex mixture of lipids, meibum melts over a temperature range of 19°C to 40°C, and not at a single temperature, so subtle alterations in composition may end upchanging meibum flow from the meibomian glands to its expression on the ocular surface, forming discontinuous tear film lipid layers[14,15,16]. Here, we propose the use of the Quartz crystal microbalance with dissipation (QMC-D) to measure the rheological properties of the lipid layer. QCM-D is a real-time, surface-sensitive technology that detects mass changes with nanoscale resolution. We can use this property to analyze interactions between molecules and surfaces, linking mass uptake or loss to a molecule's adsorption or desorption (Figure 1). Additionally, QCM-D monitors changes in energy loss, providing a valuable insight into the viscoelastic properties of the system under investigation. It can also uncover structural changes in the molecular layer at the sensor surface, such as swelling, crosslinking, and collapse. A variety of fields are increasingly adopting this technology due to its simplicity and versatility, which allows seamless integration with interface analysis devices such as electrochemistry, optical reflectometry, and scanning force microscopy. One

limitation, though, is trying to relate relevant models to experimental settings and the correlations between frequency and dissipation changes. In this work we effectively quantified the rheological properties of individual meibomian lipid samples, and we will address the significance of QCM-D as a method for analyzing films, particularly their viscoelastic properties.

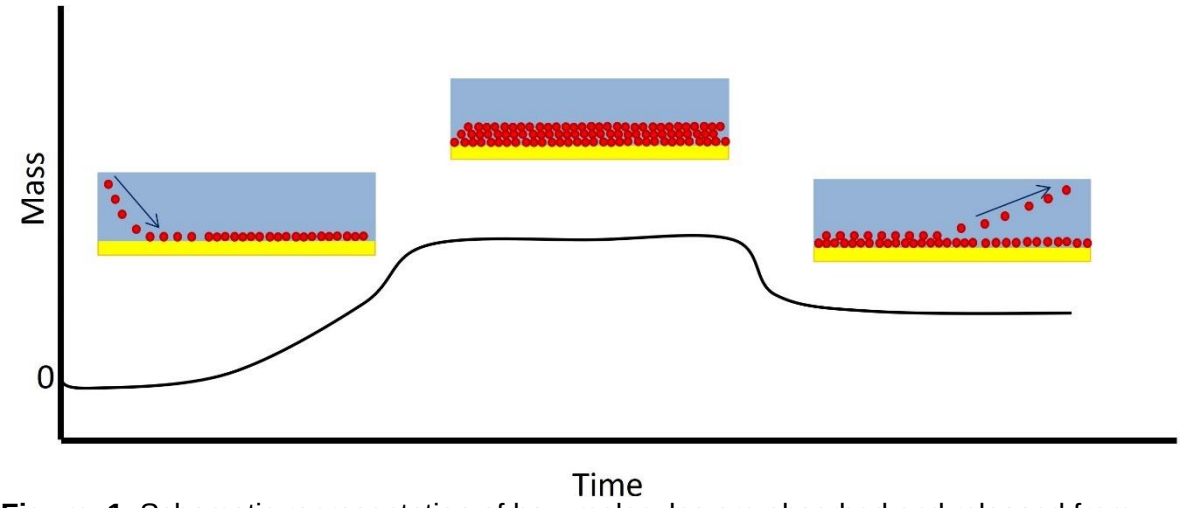

Figure 1. Schematic representation of how molecules are absorbed and released from the QCM-D sensor surface and their relationship with mass[17].

1.1 References

1. Cwiklik, L. (2016). Tear film lipid layer: A molecular level view. Biochimica Et Biophysica Acta (BBA) - Biomembranes,1858(10), 2421-2425.
2. Chhadva, P., Goldhardt, R., & Galor, A. (2017). Meibomian Gland Disease. Ophthalmology, 124(11).
3. Butovich, I. A. (2011). Lipidomics of human Meibomian gland secretions: Chemistry, biophysics, and physiological role of Meibomian lipids. Progress in Lipid Research,50(3), 278-301.
4. Nichols, K. K., Foulks, G. N., Bron, A. J., Glasgow, B. J., Dogru, M., Tsubota, K., . . . Sullivan, D. A. (2011). The International Workshop on Meibomian Gland Dysfunction: Executive Summary. Investigative Opthalmology & Visual Science, 52(4), 1922. doi:10.1167/iovs.10-6997a
5. Butovich, I. A. (2017). Meibomian glands, meibum, and meibogenesis. Experimental Eye Research,163, 2-16.
6. Georgiev, G. A., Eftimov, P., & Yokoi, N. (2017). Structure-function relationship of tear film lipid layer: A contemporary perspective. Experimental Eye Research,163,
7. King-Smith, P. E., Hinel, E. A., & Nichols, J. J. (2010). Application of a Novel Interferometric Method to Investigate the Relation between Lipid Layer Thickness and Tear Film Thinning. Investigative Opthalmology & Visual Science,51(5).
8. Green-Church, K. B., Butovich, I., Willcox, M., Borchman, D., Paulsen, F., Barabino, S., & Glasgow, B. J. (2011). The International Workshop on Meibomian Gland Dysfunction: Report of the Subcommittee on Tear Film Lipids and Lipid–Protein Interactions in Health and Disease. Investigative Opthalmology & Visual Science,52(4), 1979.
9. Millar, T. J., & Schuett, B. S. (2015). The real reason for having a meibomian lipid layer covering the outer surface of the tear film – A review. Experimental Eye Research,137, 125-138. doi:10.1016/j.exer.2015.05.002
10. Bron, A., Tiffany, J., Gouveia, S., Yokoi, N., & Voon, L. (2004). Functional aspects of the tear film lipid layer. Experimental Eye Research, 78(3), 347-360.
11. Svitova, T. F., & Lin, M. C. (2016). Dynamic interfacial properties of human tear-lipid films and their interactions with model-tear proteins in vitro. Advances in Colloid and Interface Science,233, 4-24.

12. Miljanović, B., Dana, R., Sullivan, D. A., & Schaumberg, D. A. (2007). Impact of dry eye syndrome on vision-related quality of life. American Journal of Ophthalmology, 143(3).
13. Golden MI, Meyer JJ, Patel BC. Dry Eye Syndrome. [Updated 2021 Nov 2]. In: StatPearls [Internet]. Treasure Island (FL): StatPearls Publishing; 2022 Jan-. Available from: https://www.ncbi.nlm.nih.gov/books/NBK470411/
14. Lu, H., Wojtowicz, J. C., & Butovich, I. A. (2013). Differential scanning calorimetric evaluation of human meibomian gland secretions and model lipid mixtures: Transition temperatures and cooperativity of melting. Chemistry and Physics of Lipids, 170-171, 55–64.
15. Borchman, D. (2019). The optimum temperature for the heat therapy for meibomian gland dysfunction. The Ocular Surface, 17(2), 360–364.
16. Borchman, D., Foulks, G. N., Yappert, M. C., Bell, J., Wells, E., Neravetla, S., & Greenstone, V. (2011). Human Meibum lipid conformation and thermodynamic changes with meibomian-gland dysfunction. Investigative Opthalmology & Visual Science, 52(6), 3805.
17. Butovich, I. A. (2008). On the lipid composition of human Meibum and tears: Comparative analysis of nonpolar lipids. Investigative Opthalmology & Visual Science, 49(9), 3779.
18. Adaptado de: “What is QCM-D”, por Malin Edvardsson, 2020, Biolin Scientific (https://www.biolinscientific.com/blog/what-is-qcmd).

2. Justification

Dry eye syndrome is one of the most common ophthalmologic diseases. It is a multifactorial disease resulting in tear film instability. Currently, accurate diagnosis and classification of dry eye disease is challenging due to wide variations in symptoms and the lack of a single reliable clinical assessment. In addition, changes and severity of clinical signs often do not correspond with patient-reported symptoms. Of particular interest are the meibomian lipids, which constitute the outermost layer of the tear film, as they have been identified as the determinant of its evaporative properties. Thus, meibum viscoelasticity may be a valuable indicator of how the physical properties of the meibum change and, ultimately, how they contribute to reduced tear film stability in evaporative dry eye disease. Understanding the differences in the viscoelastic properties of meibomian lipids at both the bulk and interface between healthy individuals and individuals with dry eye syndrome could be useful tools for diagnosis as well as for the development of potential treatments.

3. Objetives

3.1 General objetive

To characterize the rheological properties of meibomial lipid films from healthy individuals and patients diagnosed with dry eye syndrome in a temperature sweep.

3.2 Specific objetive

- To measure different types of materials (meibomian lipids, polydimetilsiloxane and polyethylenimine) using a QCM-D.
- To analize the data obtained using the current methods.
- To derive an algorithm for data analysis applicable to a viscoelastic layer in air, a semi infinite viscoelastic fluid, a stiff film in air, and a thin viscous film.

4. Theorethical framework

4.1 Quartz Crystal properties

In recent times, it is unthinkable a world without quartz crystals[1]. Although made from only two elements, silicon and oxygen, their applications are countless[1]. This material can be found in nature in its amorphous or in its crystalline form, yet after World War II, the demand for the creation of synthetic quartz grew as the reliance on natural quartz as the raw material for quartz products was unsustainable[1,2]. Its unique properties had allowed applications like the ones encountered in almost every electronic device with time measurement integrated, digital data processing, and wireless data transmission, among others. An interesting phenomenon found in quartz crystal that led to the development of quartz resonators is piezoelectricity, discovered in 1880 by Jacques and Pierre Curie[1,2]. Quartz crystals consist of hexagonal arrangements of silicon, which possesses a tiny positive charge, and oxygen, which has a slight negative charge, arranged so that the positive and negative centers of the resulting dipoles align[2-4]. Upon the application of a compressive force, a separation of charges occurs when the centers of positive and negative charges become misaligned, resulting in the formation of an electric field between them[2-4].This causes little voltage to be generated across it[2-4] (Figure 2). For some applications, the reverse effect is necessary, that is, crystal deformation due to an electric field, which is the physical principle of the Quartz Crystal Microbalance (QCM)[5].

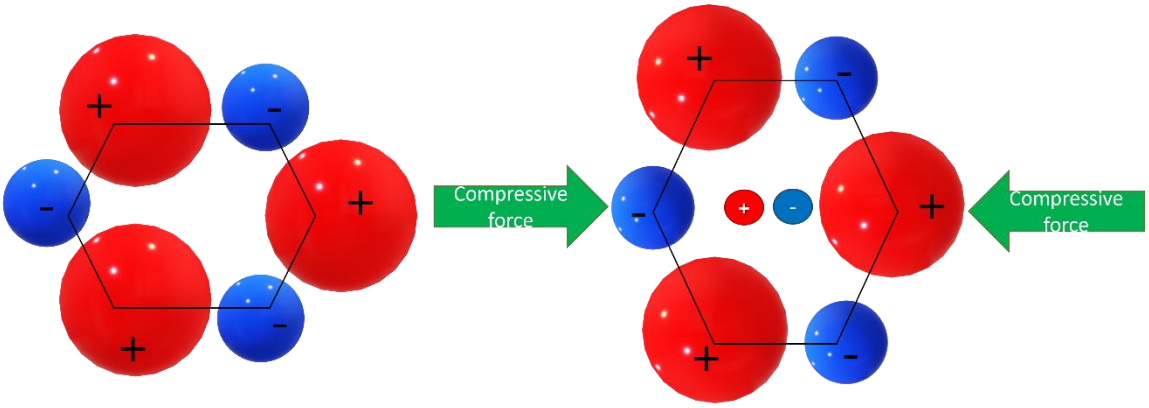

Figure 2.When a crystal undergoes deformation, causes a dipolar moment to arise on it, Hexagonal structures of silicon are shown in red and oxygen in blue[6].

When working with quartz crystal resonators, a specification that needs to be addressed is the cut[5]. Despite having a similar complex starting structure, quartz is an anisotropic material, meaning that its mechanical, electrical, and optical properties vary with direction[5]. The three primary axes of the crystal—the x, y, and z axes—are used to define the various quartz crystal cuts[5]. To achieve the necessary performance, the quartz crystal cut is essential and has a significant influence on many facets of the crystal resonator's operation[5]. Nowadays, the AT-cut quartz crystal is the most popular kind, utilized in radio systems, microprocessor clocks, electronic instruments, and a variety of other applications[7,8]. The crystal gets a cut at a ~ 35° angle measured from the z-axis (Figure 3), which gives them a low frequency-temperature coefficient, meaning their frequency is more stable in a varying temperature range compared to other cuts[7,8]. Also, only the AT- and BT-cuts oscillate in the thickness shear mode; concept we will elaborate later[7,8]. The AT cut operates at high frequencies, ranging from around 500 kHz to approximately 300 MHz. The thickness of the quartz affects frequency[7,8]. The crystal may thin down considerably at high frequencies, which leads to the top frequencies often operating in overtone mode[5].It is noteworthy that all the previously mentioned attributes make the AT crystal cut an ideal choice for mass sensing[5].

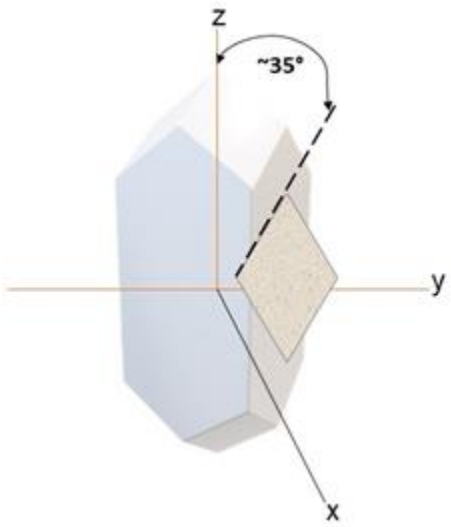

Figure 3. The various axes and faces of a quartz crystal's structure and AT cut ~35° to Z axis[9].

4.2 Anatomy of a cristal sensor

This sensor is composed of a thin AT-cut quartz substrate, typically coated with gold sheets that are bonded with chromium on both sides of the crystal[10]. The excellent conductivity and inert properties of gold make it a favored option for electrode material[11]. The electrodes imprinted on the sensor's surfaces serve dual purposes: 1) they electrically induce oscillation or resonance in the crystal, and 2) the top electrode functions as a sensing area for molecular binding[11] (Figure 4).

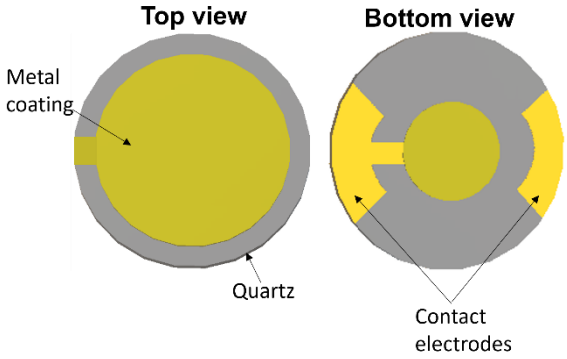

Figure 4. Schematic representation of a quartz crystal sensor[12].

The thickness shear mode appears when an oscillating electric field is applied across the sensor and a mechanical oscillation (shear deformation) is generated (Figure 5). The region that vibrates is primarily limited by the electrode overlapping. Acoustic waves are generated by deformation and propagate through the sensor

perpendicularly to the surface, with wavelengths corresponding to odd multiples of two times the thickness of the piezoelectric material, a condition necessary for crystal resonance[13-15]. However, the amplitude of crystal vibration varies across the crystal surface, influenced by the geometry of the sensor and electrodes[13-15]. Standard quartz crystal microbalances typically feature a circular electrode and a disk-shaped sensor[13-15], as illustrated in figure 4. The oscillation amplitude on these sensors exhibits a radial dependence, reaching its maximum at the center of the sensor, where the electrodes overlap, and rapidly diminishing from that point onward[13-15].

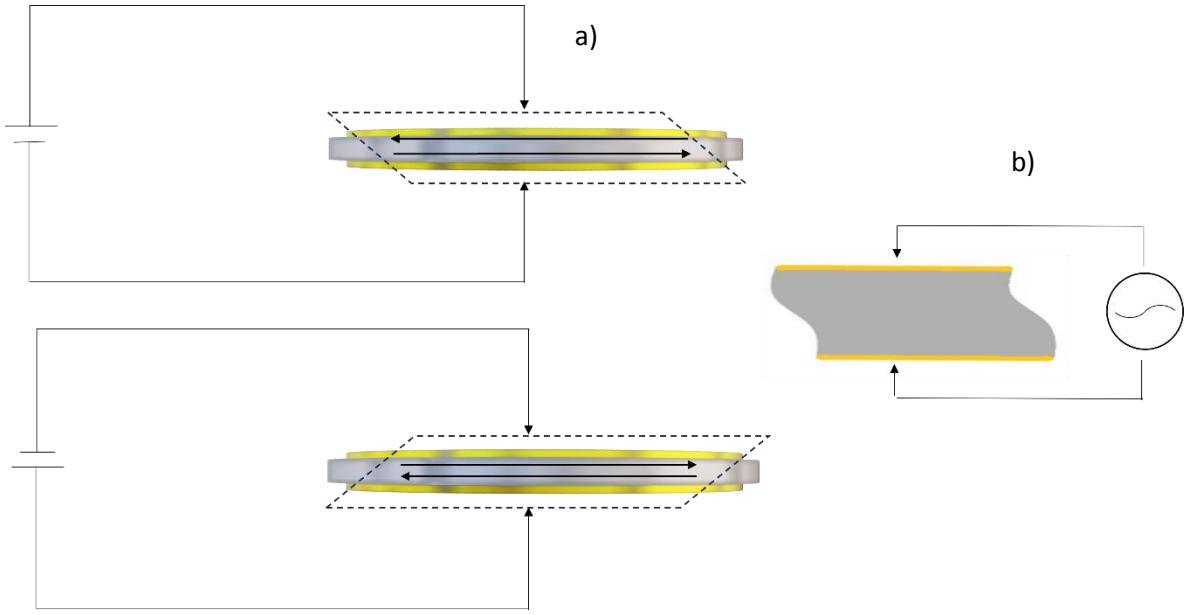

Figure 5. Thickness shear mode. a) The crystal cut and the sign of the applied voltage determines which way the deformation will go. b) For the quartz crystal sensor an alternating voltage is delivered, causing it to oscillate back and forth[16].

4.3 The quartz crystal sensor as a microbalance:Sauerbrey equation

As the name implies, the crystal sensor reacts to mass changes, becoming a gravimetric or thickness sensor, yet other parameters can be detected by the QCM, as we will elaborate later. The gravimetric sensing ability of the crystal takes the fact that the resonance frequency is dependent on the thickness of the quartz, to assume, that when a film is added to the sensing area, the crystal grows in height, yet this can also be seen as a mass addition that provokes resonance

frequency changes, for this to be fulfilled the deposited layer must be thin, rigid, evenly distributed and hold firmly to the crystal's surface (no slip condition).

As stated before, the thickness of the sensor (h_q) is an odd integer of half the wavelengths of the induced acoustic waves (λ), and can be expressed as[17]:

$$hq = n\frac{\lambda}{2} \qquad \textbf{Equation 1}$$

The relationship between the resonance frequency (f) and the wave's propagation velocity in quartz (v_q) is[17]:

$$v_q = \lambda \cdot f \qquad \textbf{Equation 2}$$

Therefore, the resonance frequency can be contained in[17]:

$$f = n\frac{v_q}{2h_q} \qquad \textbf{Equation 3}$$

Where n is the harmonic number[17]. Exclusively odd overtones are excited piezoelectrically, as a result of the formation of an equal sign surface charge on both sides of the crystal[17]. For the fundamental resonance frequency f_0, n equals 1, so equation 4 can be written as[17]:

$$f_0 = \frac{v_q}{2h_q} \qquad \textbf{Equation 4}$$

Till this point we have derived the relationship between the resonance frequency and the thickness of the quartz crystal, but for gravimetric analysis we have got to find how the frequency changes with mass[18]. We can think of the mass (M) per sensing area (A) of the quartz (m_q)as the product of thickness and density (ρ_q).[17]

$$\frac{M}{A} = m_q = h_q \cdot \rho_q \qquad \textbf{Equation 5}$$

By inserting (5) in (3) and differentiating we get[17]:

$$df = -\frac{f}{m_q} dm_q$$ **Equation 6**

If we rewrite d as Δ, and use (4) and (5), the equation transforms into[17]:

$$\Delta f = -\frac{f}{h_q \cdot \rho_q} \Delta m_q = -n \frac{2 f_0^2}{v_q \rho_q} \Delta m_q = -n \frac{1}{c} \Delta m$$ **Equation 7**

The constant c is called mass sensitivity, is determined by the mass position on the sensor's surface, it is not constant but rather has a Gaussian distribution, implicating that is constricted to the crystal's central region, therefore the significance of an evenly distributed film[18,19].

When employed for data analysis of mass determination experiments, equation 6 is used as[17]:

$$\Delta m = -c \frac{\Delta f}{n}$$ **Equation 8**

This is the well-known Sauerbrey equation establishes a linear relationship between frequency reduction and mass increment[20]. Developed in the 1950s by Günter Sauerbrey as part of his doctoral dissertation[21]. Yet, its origins can be traced to Lord Rayleigh, who contributed to the theoretical framework for utilizing quartz crystals as microbalances or detectors[22,23]. Additionally, Onoe examined the implications of surface coatings on quartz crystals[24]. However, it was Sauerbrey who formalized this empirical knowledge into an equation and an instrument[21]. For a long time, people primarily used QCM technology to weigh samples, treating them as a crystal extension, and measuring them in air or vacuum. However, many reactions and possible future uses happen in liquids or with materials that are viscoelastic.

4.4 QCM measurements in liquid

Despite some thought impossible due to damping of the acoustic waves, in the 80's Konash and Bastiaans made the initial attempt to use the piezoelectric quartz crystal as a liquid phase sensor, with little success[25,26]. During that same period, Nomura studied mass transfer during electrodeposition, while Bruckenstein and Shay combined a QCM with an electrochemical cell[26,27]. In most studies that used the QCM as a mass sensor, only the resonance frequency was measured[28]. The Sauerbrey equation was used to estimate the amount of mass that had built up on the QCM electrode, but this could lead to a wrong result because it is based on a number of assumptions that might not hold true if certain conditions are not met[28]. The liquid itself has an effect; the Kanazawa-Gordon equation, as it is currently known, describes this impact, while the Sauerbrey equation simply considers the properties of quartz. The Kanazawa-Gordon equation states that the quartz frequency diminution is a result of liquid damping proportional to the liquid's viscosity η_L and density ρ_L[29].

$$\Delta f_{Liquid} = -f_0^{3/2} \frac{\sqrt{\eta_L \rho_L}}{\pi \mu_q \rho_q} \qquad \textbf{Equation 9}$$

Where μ_q is the quartz shear modulus[29]. The non-slip boundary condition at the liquid-solid interface draws the liquid at the surface closer to the QCM sensor[29]. The shear motion of the crystal surface creates a shear wave that permeates the liquid; this produces a velocity profile that can be explained by the Navier-Stokes equation[28,30]. Before entirely losing its energy, the shear wave travels a distance known as the penetration depth into the liquid layer; the liquid's viscosity causes the wave's energy to dissipate exponentially[28,30] (Figure 6).

$$\delta = \sqrt{\frac{2\eta_L}{\omega \rho_L}} \qquad \textbf{Equation 10}$$

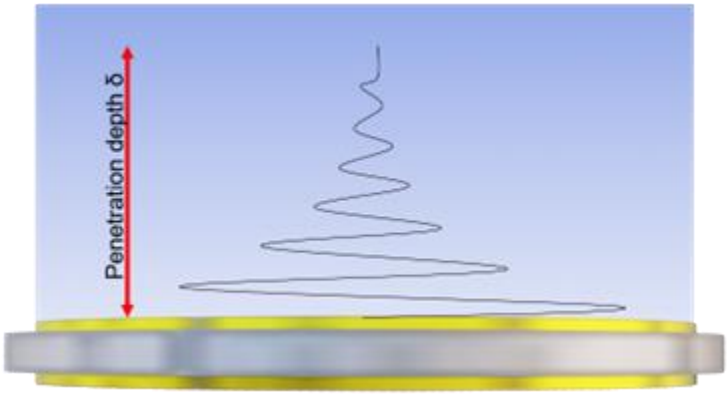

Figure 6. The penetration depth is the maximum distance a wave can travel through a liquid. It is shown that the amplitude of the shear wave significantly attenuates[31].

For a shear acoustic wave generated by a 5-MHz crystal that is propagating in water the penetration depth is 250 nm, a more viscous fluid like glycerol will allow the shear wave to enter deeper[30]. The dependence of the decay length on the sensor resonance frequency is another significant result of Equation that has broad practical implications[30]. This allows for probing at various distances from the sensor surface, allowing one to measure at the sensor overtones and obtain information about various layers[30].

4.5 Energy losses, QCM-D and QCM-I

As was discussed in the previous section, within the film, internal friction results in energy loss due to viscosity-induced oscillatory motion, additionally, frictional energy is dissipated if the film slips on the electrode[30,32]. Measuring energy losses in addition to the resonance frequency can provide further insight about the characteristics of the material on the resonator's surface[30,32]. The simplest version of the QCM form consists of a Quartz crystal integrated into the feedback network of an oscillator circuit, where the output frequencies are monitored[33-36]. The Butterworth van Dyke equivalent circuit can be used to represent of the unloaded QCM's equivalent circuit, as shown on the figure 7, it is formed by a shunt capacitance(C_0) in parallel with an inductance (L_1), a capacitance (C_1), and a resistance (R_1)[33-36] . R_1 is a representation of the energy lost by the medium in contact with the quartz sensor and the mounting structures, elasticity of the quartz

crystal and the media surrounded by it are related to C_1, which is the oscillation stored energy, L_1 is linked to the mass displaced during the vibration and represents the mass, and the total static capacitance of the crystal electrodes, holder, and connector is shown in C_0[33-36].

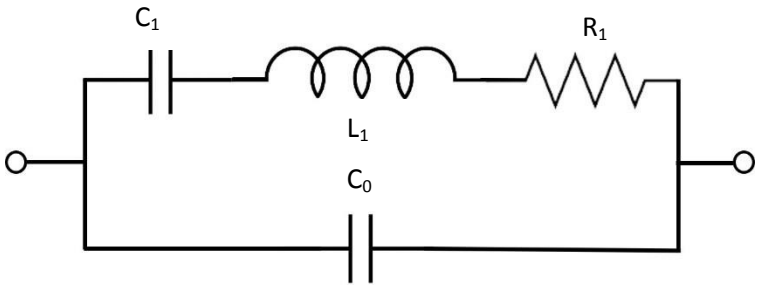

Figure 7. Butterworth-van-Dyke equivalent circuit[37].

Basic oscillator circuits only yield the resonance frequency, but a network analyzer can also register the impedance of the quartz crystal[21,27,33]. The impedance analyzer determines the resonator's electrical admittance by sweeping the frequency across the resonance; at this frequency the conductance G_{el} has a maximum. By measuring the half bandwidth at half maximum (usually just referred to as half bandwidth or bandwidth) Γ of this resonance, peak energy lost is captured; this method is called impedance analysis[21,27,33]. The resonant frequency of a clean sensor, measured in air, corresponds to the maximum conductance; however, upon loading a sample onto the sensor's surface, the frequency diminishes and the peak moves[21,27,33] (Figure 8).

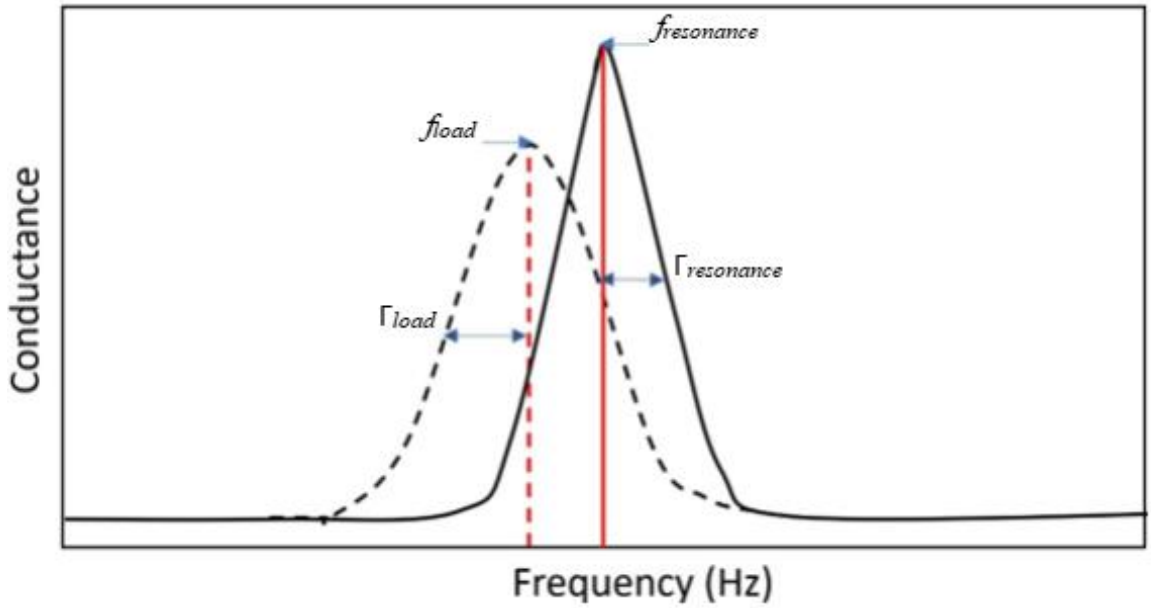

Figure 8. Exemplary signals obtained from impedance analysis in experiments[38].

Rodahl et al. introduced the dissipation monitoring with ring down method (also known as impulse excitation or pinning) in 1995[33]. Biolin scientific is the company that commercializes this method under the name QCM-D. A computer-controlled relay is employed to intermittently detach the oscillating crystal from the drive circuit, facilitating dissipation and frequency measurements[21,32]. As a result, the driver circuit is disconnected and the amplitude of the crystal oscillation dies off exponentially over time, using a high-impedance probe, the decay of the QCM oscillation is captured on a digitizing oscilloscope, after that, the decay curve is loaded onto a computer, where it is numerically fitted to the equations[21,27,32,33] (Figure 9).

$$q(t) = A_0 e^{\frac{-t}{\tau}} \sin(\omega t + \phi), t \geq 0 \qquad \textbf{Equation 11}$$

$$D = \frac{1}{\pi f \tau} \qquad \textbf{Equation 12}$$

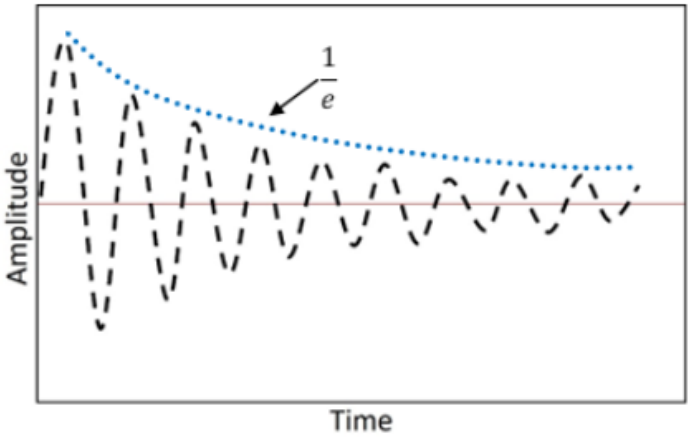

Figure 9. The energy dissipation D and the resonance frequency f are taken from the decay curve[39].

From now on, when talking about energy loss measurements, we will use the term, dissipation, as the equipment used during this work was a QCM-D, yet dissipation and half bandwidth are linked through equation[21,27]:

$$D = \frac{2\Gamma}{f}$$ **Equation 13**

4.6 Viscoelastic analysis

4.6.1 Kelvin-Voigt model

Although QCM experiments and qualitative examination of data may be quite simple, when dealing with viscoelastic materials, data analysis and interpretation turn into a challenge[40]. The go-to method for QCM-D data analysis is the Kelvin-Voigt model, especially when measuring with Biolin scientific apparatus, as it is the analysis software's default setting[41]. This method is attributed to Voinova et al.[41], It assumes a continuum model that describes the viscoelastic response to shear deformation of two slices with specific density (ρ_1, ρ_2), thickness (h_1, h_2), viscosity (η_1, η_2), and elasticity (μ_1, μ_2), that are submerged in a bulk newtonian liquid (ρ_3, η_3)[40,41] (Figure 10).

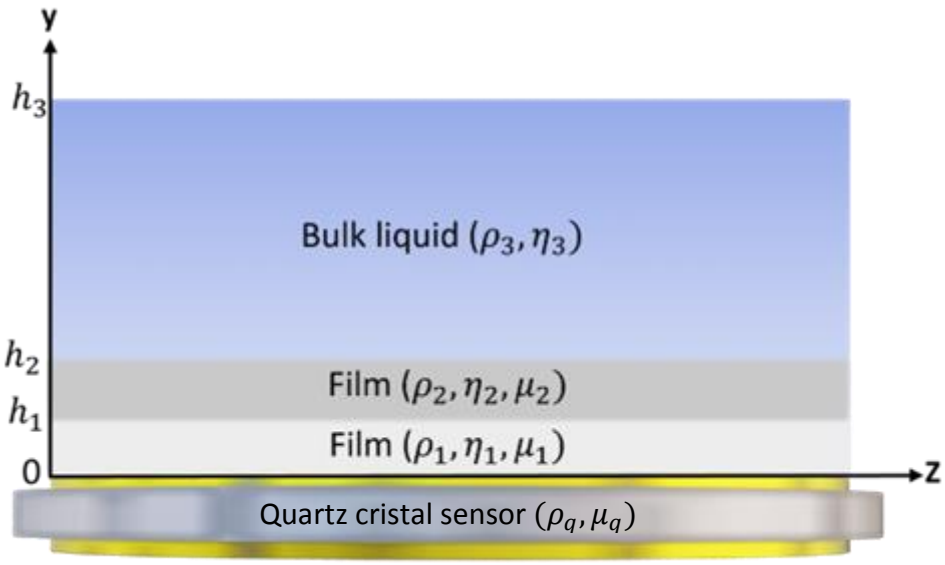

Figure 10. Voinova's model for viscoelastic analysis[42].

A general solution for the wave equation that describes how shear waves travel from the quartz sensor through a layered viscoelastic medium within the Kelvin-Voigt scheme (Figure 11) and eventually fade[41]. The solution is derived considering no-slip boundary conditions; from that, the change in frequency and dissipation come from both the imaginary and real components of the beta function, respectively[41].

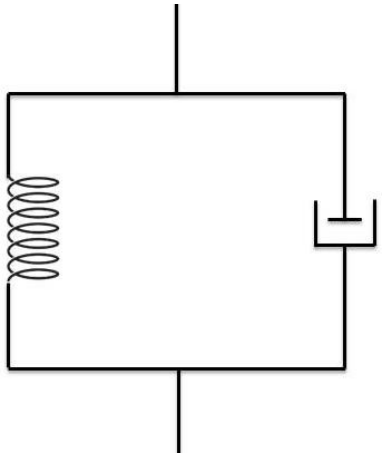

Figure 11.Schematic represantation of the Kelvin-Voigt viscoelastic element, consisting in a spring and a dashpot in parallel[42].

This model offers solutions for the limit cases of thin and thick viscoelastic layers placed on the quartz oscillator surface in two different environments, one being a gaseous environment and the other being a bulk liquid are provided[41]. For two thin

viscoelastic layers of thickness h_1 and h_2 immersed in a Newtonian liquid with index 3. The difference in frequency and dissipation are[41]:

$$\Delta f \approx -\frac{1}{2\pi\rho_q h_0}\left\{\frac{\eta_3}{\delta_3}+\sum_{j=1,2}\left[h_j\rho_j\omega-2h_j\left(\frac{\eta_3}{\delta_3}\right)^2\frac{\eta_j\omega^2}{\mu_j^2+\omega^2\eta_j^2}\right]\right\} \quad \textbf{Equation 14}$$

$$\Delta D \approx -\frac{1}{2\pi f\rho_q h_0}\left\{\frac{\eta_3}{\delta_3}+\sum_{j=1,2}\left[2h_j(\frac{\eta_3}{\delta_3})^2\frac{\mu_j\omega}{\mu_j^2+\omega^2\eta_j^2}\right]\right\} \quad \textbf{Equation 15}$$

According to Voinova et al. this model can be applied with polymer brushes or polymer films away from the glass transition region and protein films in situations where the proteins maintain their structure and are static under shear deformation[41]. This model is not appropriate for discrete particles since it requires a uniform film[40]. Another one of its drawbacks is that the viscoelastic element is characterized by the complex shear modulus, whose real portion (storage modulus) is frequency independent while its imaginary portion (loss modulus) raises linearly with frequency, which is typically unjustified, as the Kelvin Voigt range is completely absent for most materials that are of interest[40,41]. Moreover, other than coincidence, this frequency range is unlikely to correspond with the frequencies covered by QCM in practice[40]. In addition to the Kelvin Voigt method, there is another approach that is widely used in literature to determine the frequency shift caused by a viscoelastic layer in a fluid; the small-load approximation[43]. The two approaches are interchangeable despite the languages are different[43]. While the Kelvin Voigt model uses the wave equation, the small-load approximation uses acoustic terminology[43].

4.6.2 Small-load approximation

At resonance, the crystal experiences a force from the sample that is counteracted by a force generated by the shear gradient within the crystal[43]. This encapsulates the fundamental concept of the small-load approximation. In the small-load approximation (SLA), the quartz crystal sensor is defined as a laterally infinite plate that experiences motion in the thickness-shear direction, with the sample on top acting as a load[21,27,43]. The modeling of this arrangement can be done using the BVD circuit, relating the frequency shift due to the load and the stress-speed ratio of the quartz sensor surface and the sample, also known as the load impedance, Z_L[43]. The frequency shift can be estimated as:

$$\frac{\Delta f^*}{f_0} = \frac{i}{\pi}\frac{Z_L}{Z_q}$$ **Equation 16**

Where Δf^* is the complex frequency shift that is equal to $\Delta f + i\Delta\Gamma$. The SLA's applicability necessitates $|\Delta f \ll f_0|$, as well as a Z_L smaller than the AT-cut quartz's acoustic impedance, Zq, as the name implies[43]. Most practical cases fulfill this last requirement. We have not yet made any declarations about the sample's nature. This equation enables the calculation of frequency shifts for a wide range of materials, even heterogeneous ones[40]. If it is possible to quantify the stress-velocity ratio of the sample, a quantitative analysis of the QCM can be employed[43]. There are specific formulas that connect Δf^* to the properties of the sample for various configurations. By assuming that the sensor and the layers covering it are infinite and laterally homogenous and that every stress is directly proportional to its corresponding strain, the concept of linear viscosity remains valid[21,27,43]. For example, one can derive Sauerbrey equation from SLA, if a rigid material is placed on top of the sensor, the stress is determined by inertia, so the load impedance is[21,27,43]:

$$Z_L = \frac{\hat{\sigma}_S}{\hat{V}_S} = \frac{-\omega^2 \hat{u}_S m}{i\omega \hat{u}_S} = i\omega m$$ **Equation 17**

Where $\hat{\sigma}_S$ is the stress, $\hat{V}_S$ the velocity and $\hat{u}_S$ the displacement and at the surface. When this load is inserted into the SLA[21,27,43]:

$$\frac{\Delta f^*}{f_0} \approx \frac{i}{\pi Z_q} i\omega m = -\frac{2nf_0}{Z_q} m = -n\frac{m}{m_q}$$ **Equation 18**

SLA can be applied to viscoelastic materials. When dealing with a semi-infinite viscoelastic medium[43]:

$$\frac{\Delta f^*}{f_0} = \frac{i}{\pi Z_q} Z_{ac} = \frac{i}{\pi Z_q}\sqrt{i\rho\omega\eta} = \frac{i}{\pi Z_q}\sqrt{\rho(G' + iG'')}$$ **Equation 19**

$\eta = \eta' - i\eta''$ is the complex shear viscosity, $G = i\omega\eta$ is the complex shear modulus, and $Z_{ac} = \rho c = \sqrt{G\rho}$ is the acoustic impedance of the medium[43]. For Newtonian liquids Δf and $\Delta\Gamma$ are equal and opposite ($\eta' = constant, \eta'' = 0$)[43]. For non-Newtonian liquids ($\eta' = \eta(\omega)$, $\eta'' \neq 0$), the complex viscosity from QCM data can be derive through the following equations[43]:

$$\eta'' = \frac{G''}{\omega} = -\frac{\pi Z_q^2}{\rho_L f}\frac{\Delta f \Delta\Gamma}{f_0^2} \qquad \textbf{Equation 20}$$

$$\eta'' = \frac{G'}{\omega} = -\frac{1}{2}\frac{\pi Z_q^2}{\rho_L f}\frac{(\Delta\Gamma^2 - \Delta f^2)}{f_0^2} \qquad \textbf{Equation 21}$$

The frequency shift generated by placing a thin viscoelastic layer on top of the quartz sensor can be calculated when measured in air as[43]:

$$\frac{\Delta f^*}{f_0} \approx \frac{-1}{\pi Z_q}\omega m_{film}\left[1 + \frac{(n\pi)^2}{3}\frac{Z_q^2}{Z^{*2}_{film}}\left(\frac{m_{film}}{m_q}\right)^2\right] \qquad \textbf{Equation 22}$$

Where Z^*_{film} is the acoustic impedance of the film. When measuring thin films in air, a two-part equation is utilized. This equation consists of the Sauerbrey equation and a viscoelastic correction[21,27,43]. Equations have been derived specifically for other certain instances; another involves a viscoelastic film that is measured while being submerged in a liquid. In this case, the equation is equivalent to the Kelvin-Voigt model[21,27,43]. The concept of load impedance significantly broadens the scope of applications for the quartz crystal microbalance, making its use more common in various fields. It is commonly used among other instruments in many articles to analyze samples.

4.6.3 Power-law model

Shull and colleagues developed another method for determining viscoelastic properties that is based on a self-consistent description of the complex modulus[44]. It is a more universally applicable model in which the storage and loss moduli are

both assumed to follow power-law functions based on the frequency, and the phase angle is directly connected to the value of the power-law exponent[44]. The power-law model is more straightforward to use and has minimal impact on the accuracy of the physical properties obtained from a properly constructed QCM experiment[44,45]. We have already mentioned that in the case of attached layers that are sufficiently rigid and/or thin, the frequency of the material will be directly proportional to its mass, according to the Sauerbrey expression[44]. As a result, the material's viscoelastic properties are not necessary to describe the QCM's function[44,45]. Yet, when there are deviations from Sauerbrey regime viscoelastic characterization is allowed[44,45]. The point at which the Sauerbrey expression fails to accurately quantify can be defined in relation to $\frac{h_{film}}{\lambda_n}$, which is the ratio of the film thickness by the shear wavelength of the mechanical oscillation at the n overtone in a medium and ϕ that is the viscoelastic phase angle of the medium[44,45]. λ_n is determined by the following expression[44,45]:

$$\lambda_n = \frac{1}{f_n}\left[\frac{|G_n^*|}{\rho}\right]\frac{1}{\cos(\frac{\phi}{2})} \qquad \textbf{Equation 23}$$

Where $|G_n^*|$ is the magnitude of the complex shear modulus at the n overtone[44,45]. The shear wave propagation in a medium can be described using three distinct limiting situations[44,45]. If the film is of sufficient thickness, the shear wave dissipates entirely within the adhering layer of the material[44,45]. This situation can be regarded as being analogous to the bulk measurement of the material, where the fluid film thickness does not influence the response[44,45]. The following two equations describe the QCM response in this limit[44,45]:

$$\Delta f_n = \frac{-f_1}{\pi Z_q}(\rho|G_n^*|)^2\sin(\frac{\phi}{2}) \qquad \textbf{Equation 24}$$

$$\Delta \Gamma_n = \frac{f_1}{\pi Z_q}(\rho|G_n^*|)^2\cos(\frac{\phi}{2}) \qquad \textbf{Equation 25}$$

A more typical scenario occurs when the shear wave travels through the attached layer and then completely dissipates in the surrounding liquid, resulting in both the film and the liquid phase contributing to the crystal's reaction[44,45]. When a shear wave reaches the boundary between the film and liquid, it separates into a transmitted wave and a reflected wave[44,45]. The reflected wave typically causes a slight reduction in the oscillation frequency detected by the sensor[44,45]. Nevertheless, it is feasible for the reflected shear wave to combine with the outbound shear wave, resulting in an augmented oscillation frequency at the sensor surface due to the combined effect of these two transverse waves[44,45]. Film resonance refers to the specific condition in which the shear wave becomes coupled with the reflected wave[44,45]. The response of the QCM can be described by the following equation[44,45]:

$$\frac{\Delta f_n^*}{\Delta f_{sauerbrey}} = -\frac{\tan(D_{nfilm}^*)}{D_{nfilm}^*}\left[\frac{1-(r^*)^2}{1+ir^*\tan(D_{nfilm}^*)}\right] \quad \textbf{Equation 26}$$

Where r^* is:

$$r^* = \left(\frac{\rho_{liquid}G_{liquid}^*}{\rho_{film}G_{film}^*}\right) \quad \textbf{Equation 27}$$

and D_{nfilm}^* is:

$$D_{nfilm}^* = \frac{2\pi d}{\lambda_n}(1 - itan\left(\frac{\phi_n}{2}\right)) \quad \textbf{Equation 28}$$

It becomes evident that there is no overall reaction when the film and liquid medium have the same properties (r* = 1), and that the QCM response for a film in air is restored when r* = 0[43]. For this model to be applied it is neccesary to measure frequency and dissipation at two harmonics, so the ratios $\frac{n_2\Delta f_{n_1}}{n_1\Delta f_{n_2}}$ and $\frac{\Delta\Gamma_{n_3}}{\Delta f_{n_3}}$ are calculated using the equations, with ϕ_n and $\frac{h_{film}}{\lambda_n}$as the unknown values, to

make them agree with the experimental values[47]. Once $\frac{h_{film}}{\lambda_n}$ is found, the product from the density and thickness of the film can be determined, to lastly determine the product $|G_1^*|\rho$[46]. This brief summary demonstrates the various ways to translate the data (Δf and ΔD) from the QCM into the viscoelastic properties of the measured films. Despite the apparent differences between these approaches, you can use Johannsmann's proposal to derive the Voinova and Shull and coworkers methods. With Biolin Scientific's popularization and commercialization of the QCM, the Voinova model gained popularity, but it has the drawback of requiring a priori selection of either Maxwell or Kelvin Voight as the model in order to analyze the data. Additionally, researchers have found that the Voigt model can provide modulus and phase angles, even in the Sauerbrey limit, where the QCM response lacks viscoelastic information[44]. In this work we derive a general equation based in Johannsmann approach combining it with Voinova lenguaje. The next chapter will have this equation with some especific cases, and some tips and tricks in the use of the QCM.

4.7 References

1. Büchler, C. y Laskus, M. (2020). Quartz crystal in theory and practice. www.jauch.com
2. Yoshimura, J.-I. (2023). Production and Applications of Synthetic Quartz. IntechOpen. doi: 10.5772/intechopen.111593
3. Arnau, A. (2004). *Piezoelectric transducers and applications*. Springer.
4. Bunde, R. L., Jarvi, E. J., & Rosentreter, J. J. (1998). Piezoelectric Quartz Crystal Biosensors. *Talanta*, *46*(6), 1223–1236.
5. Notes, E. (n.d.). *Quartz Crystal Cuts: At, bt, SC, CT . .* Electronics Notes. https://www.electronics-notes.com/articles/electronic_components/quartz-crystal-xtal/crystal-resonator-cuts-at-bt-sc-ct.php#google_vignette
6. Adaptado de: "Piezoelectric material" , 2020, Audiowell Sensor technology (https://www.audiowell.com/technology/186.html).
7. Zafirah, T. N., Triqadafi, A. O., Kusuma, F. J., & Sakti, S. P. (2021). Frequency response of quartz crystal microbalance under Uniaxial Force. *Journal of Physics: Conference Series*, *1951*(1), 012041.
8. Ward, M. D., & Buttry, D. A. (1990). In situ interfacial mass detection with piezoelectric transducers. *Science*, *249*(4972), 1000–1007.
9. Adaptado de: "Quartz Crystal Cuts: AT, BT, SC, CT . ." , por Ian Poole, 2020, electronicsnotes (https://www.electronics-notes.com/articles/electronic_components/quartz-crystal-xtal/crystal-resonator-cuts-at-bt-sc-ct.php).
10. Richardson, A., Bhethanabotla, V. R., Smith, A. L., & Josse, F. (2009). Patterned electrodes for thickness shear mode quartz resonators to achieve uniform mass sensitivity distribution. *IEEE Sensors Journal*, *9*(12), 1772–1777.
11. Surface plasmon resonance vs. Quartz Crystal Microbalance. (n.d.). https://biosensingusa.com/wp-content/uploads/2015/03/TechnicalNote103-Surface-Plasmon-Resonance-vs.-Quartz-Crystal-Microbalance.pdf
12. Adaptado de: "What is Quartz Crystal Microbalance (QCM)?", 2020, nanoscience instruments (https://www.nanoscience.com/techniques/quartz-crystal-microbalance/).
13. Martin, S. J., Granstaff, V. Edwards., & Frye, G. C. (1991). Characterization of a quartz crystal microbalance with simultaneous mass and liquid loading. *Analytical Chemistry*, *63*(20), 2272–2281.
14. HEN, D., KANG, Q., WANG, Y., HU, Q., & DU, J. (2008). New Cut Angle quartz crystal microbalance with low frequency–temperature coefficients in an aqueous phase. *Talanta*, *76*(4), 803–808.
15. Granstaff, V. E., & Martin, S. J. (1994). Characterization of a thickness-shear mode quartz resonator with multiple nonpiezoelectric layers. *Journal of Applied Physics*, *75*(3), 1319–1329.
16. Adaptado de: "Exploring QCM Technology: How Quartz Crystal Microbalance Works", por Malin Edvardsson, 2024, Biolin Scientific (https://www.biolinscientific.com/blog/how-does-qcm-technology-work).
17. The Sauerbrey equation. (n.d.). https://www.biolinscientific.com/hubfs/Content Offer/QSense/EN/The Sauerbrey relation v2.pdf?hsLang=en
18. Hu, J., Huang, X., Xue, S., Yesilbas, G., Knoll, A., & Schneider, O. (2020). Measurement of the mass sensitivity of QCM with ring electrodes using electrodeposition. *Electrochemistry Communications*, *116*, 106744.

19. Cumpson, P. J., & Seah, M. P. (1990). The quartz crystal microbalance; radial/polar dependence of mass sensitivity both on and off the electrodes. *Measurement Science and Technology*, *1*(7), 544–555.
20. Higuchi, R., & Kanno, Y. (2006). New analysis from the strength of materials of Sauerbrey's equation concerning the quartz crystal microbalance. *Japanese Journal of Applied Physics*, *45*(5R), 4232.
21. Johannsmann, D., Langhoff, A., & Leppin, C. (2021). Studying soft interfaces with shear waves: Principles and applications of the Quartz Crystal Microbalance (QCM). *Sensors*, *21*(10).
22. J.W. Strutt (Lord Rayleigh), The Theory of Sound, rev. ed., Dover, NY, 1945, p. 117.
23. Lu, C., & Czanderna, A. W. (1984). *Applications of piezoelectric quartz crystal microbalances*. Elsevier.
24. M. Onoe, Proc. IRE, 45 (1957) 694
25. Kankare, J. (2002). Sauerbrey equation of quartz crystal microbalance in liquid medium. *Langmuir*, *18*(18), 7092–7094.
26. Čavić-Vlasak, B. A., & Rajaković, L. J. (1992). Application potential of liquid-phase acoustic wave devices as chemical and biochemical sensors. *Fresenius' Journal of Analytical Chemistry*, *343*(4), 339–347.
27. Johannsmann, D. (2015). *Quartz Crystal Microbalance in soft matter research: Fundamentals and modeling*. Springer International Publishing
28. Rickert, J., Brecht, A., & Göpel, W. (1997a). QCM operation in liquids: constant sensitivity during formation of extended protein multilayers by affinity. *Analytical Chemistry*, *69*(7), 1441–1448.
29. Keiji Kanazawa, K., & Gordon, J. G. (1985). The oscillation frequency of a quartz resonator in contact with liquid. *Analytica Chimica Acta*, *175*, 99–105.
30. Ferreira, G. N. M., da-Silva, A.-C., & Tomé, B. (2009). Acoustic wave biosensors: Physical models and biological applications of Quartz Crystal Microbalance. *Trends in Biotechnology*, *27*(12), 689–697.
31. Adaptado de: "Modeling the response of a quartz crystalmicrobalance under nanoscale confinement andslip boundary conditions" (p. 7225), por Xiaoxi Qiao, Xiangjun Zhang, Yu Tian and Yonggang Meng, 2015, Physical Chemistry Chemical Physics, 3(3).
32. Rodahl, M., & Kasemo, B. (1996). On the measurement of thin liquid overlayers with the quartz-crystal microbalance. *Sensors and Actuators A: Physical*, *54*(1–3), 448–456.
33. Zhang, Y., Du, B., Chen, X., & Ma, H. (2008a). Convergence of dissipation and impedance analysis of Quartz Crystal Microbalance Studies. *Analytical Chemistry*, *81*(2), 642–648.
34. Tumurbaatar, B., Kim, M.-J., Park, C.-H., & Kim, C. S. (2018a). A portable and computer-simulation analysis for the real-time measurement of the QCMD systems for the Biomedical Application. *Sensing and Bio-Sensing Research*, *21*, 75–81.
35. Fort, A., Panzardi, E., Vignoli, V., Tani, M., Landi, E., Mugnaini, M., & Vaccarella, P. (2021). An adaptive measurement system for the simultaneous evaluation of frequency shift and series resistance of QCM in liquid. *Sensors*, *21*(3), 678.
36. Burda, I. (2022). Quartz crystal microbalance with impedance analysis based on virtual instrumen: Experimental study. *Sensors*, *22*(4), 1506.
37. Adaptado de: "Analysis and equivalent circuit for accurate wideband calculations of the impedance for a piezoelectric transducer having loss" (p. 4), por M. J. Hagmann, 2019, AIP Advances, 9(8).

38. Adaptado de: “The Principles of QCM-IQ”, por M. J. Swann, 2020, GamryInstruments (https://www.gamry.com/application-notes/qcm/qcm-i-principles/).
39. Adaptado de: “Different methods for measuring Dissipation in QCMs and why they matter”, por Malin Edvardsson, 2024, Biolin Scientific, (https://www.biolinscientific.com/blog/different-ways-of-measuring-the-dissipation).
40. Reviakine, I., Johannsmann, D. and Richter, R.P. (2011) ‘Hearing what you cannot see and visualizing what you hear: Interpreting quartz crystal microbalance data from solvated interfaces’, *Analytical Chemistry*, 83(23), pp. 8838–8848.
41. Voinova, M. V., Rodahl, M., Jonson, M., & Kasemo, B. (1999, May 1). Viscoelastic Acoustic Response of Layered Polymer Films at Fluid-Solid Interfaces: Continuum Mechanics Approach. *Physica Scripta*, *59*(5), 391–396.
42. Adaptado de: “Viscoelastic Acoustic Response of Layered Polymer Films at Fluid-Solid Interfaces: Continuum Mechanics” (p. 392), por Voinova, M. V., Rodahl, M., Jonson, M., & Kasemo, B., 1999, Physica Scripta, 59(5).
43. Johannsmann, D. (2008). Viscoelastic, mechanical, and dielectric measurements on complex samples with the Quartz Crystal Microbalance. *Physical Chemistry Chemical Physics*, *10*(31), 4516.
44. Sadman, K., Wiener, C. G., Weiss, R. A., White, C. C., Shull, K. R., & Vogt, B. D. (2018). Quantitative rheometry of thin soft materials using the quartz crystal microbalance with dissipation. Analytical Chemistry, 90(6), 4079–4088.
45. Shull, K. R., Taghon, M., & Wang, Q. (2020). Investigations of the high-frequency dynamic properties of polymeric systems with quartz crystal resonators. Biointerphases, 15(2).
46. DeNolf, G. C., Haack, L., Holubka, J., Straccia, A., Blohowiak, K., Broadbent, C., & Shull, K. R. (2011). High frequency rheometry of viscoelastic coatings with the Quartz Crystal Microbalance. *Langmuir*, *27*(16), 9873–9879.

5. Methodology: Tips and tricks for experimental design and data analysis

This section will be dealing with the experimental design. As any experiment's main objective is to provide information, we believe that effective data analysis begins in the laboratory. Although QCM experiments are easy to perform, there are some key considerations to make; they will be listed here. Also, we will be discussing data acquisition and analysis. As previously stated, numerous methods exist for determining viscoelastic characteristics; however, we propose an alternative strategy that integrates both the Voinova and Johannsmann methodologies to simplify the process.

5.1 Cleaning the sensor

When dealing with the interaction of samples with surfaces, cleanliness is critical, especially on a sensitive device that can detect samples in the order of nanograms. As a result, to obtain reproducible measurements, proper cleaning and surface preparation procedures must be followed. The optimal cleaning technique is reliant upon the characteristics of the sample system, the manner in which the sample interacts with the sensor surface, and the features inherent to the sensor[1]. Before every experiment, the gold-covered sensor is cleaned on a heated 5:1:1 $H_2O/H_2O_2/NH_4O$ mixture for 10 minutes, and finally, rinsed thoroughly with deionized water and dried with nitogen gas[2].

5.2 The good practice of measuring the bare sensor in air

After the cleaning procedure, it is necessary to start any experiment with a measurement of the bare sensor in air, as we are measuring how frequency decreases due to sensor loading or depending on the material, if there is any increase in dissipation. One would anticipate these reference values to remain constant over time, the so-called stable baseline (Figure 11a) it is crucial to wait until the baseline is stable before depositing any samples[3]. Under favorable conditions, the sensor can be reused up to 30 times[1]. Nevertheless, it necessitates meticulous handling and cleaning protocols avoiding any damage to the sensor or its coating[1]. Although visual examination frequently reveals indications of usage and deterioration, the sensor may fracture, and the coating may exhibit abrasion and holes that could be seen while examining frequency and dissipation data. The measured signal will see an increase in noise and may even exhibit instability as the sensor approaches the end of its lifespan. Acquiring a consistent, stable baseline could potentially be difficult. Usually, even if sensors are clean, they experience a little deviation from the baseline, called drift[3,4] (Figure 11b). For a clean 5 MHz sensor at 25°C and recorded at the third harmonic, a normal frequency and dissipation drift is of less than 2 Hz/h and 2x10-7/h in water[3,4]. When it comes to air, the drifts are typically larger because there are slower fluctuations in factors such as humidity[3,4]. A larger-than-expected drift could make more difficult to reach a stable baseline. There are many reasons to why this happens, among the potential ones are: temperature changes, unexpected surface responses and mounting stresses[3,4].

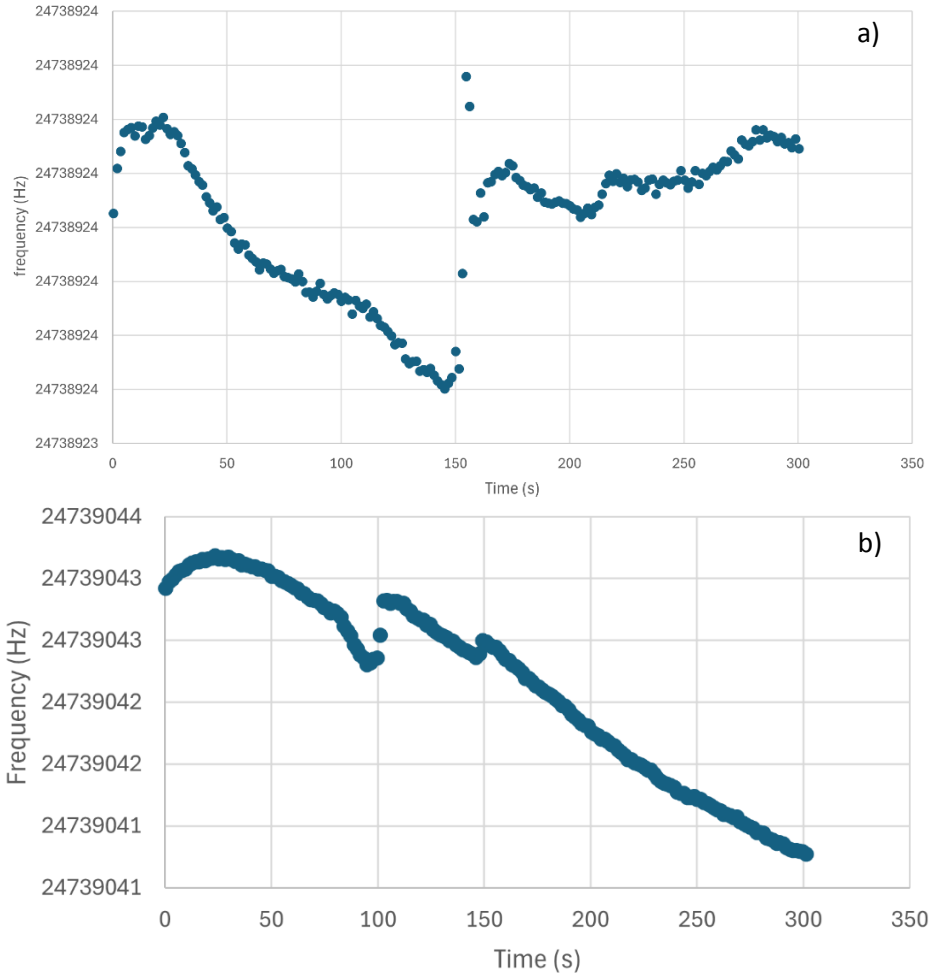

Figure 12. Baseline in air. We see the frequency drift of the 5th overtone, in a) a non-viable air measurement, check for temperature changes, mounting stresses or look up for damage in the sensor. b) a perfect measurement in air, with minimal drift.

5.3 How to recover the mesured data

One of the first challenges we encounter with the QCM-D is that the data could only be accessed using the QTools software, so after the experiment is completed a file with a .QSD extension is generated. Once the file is opened, the data from the experiment is shown as:

$$Displayed\ frequency\ value = \frac{(real\ value - offset)}{overtone} \qquad \textbf{Equation 29}$$

$$Displayed\ Dissipation\ value = \frac{(real\ value - offset)}{(1 \times 10^{-6})}$$ **Equation 30**

The file could be exported either as an ASCII or Excel file. In order to make the analysis, the real frequency and dissipation value is needed, so it is important to save in a separate text file the row labeled as offset, as it will not be shown on the exported data file.

5.4 Calibration

By conducting measurements in air, we may obtain crucial data regarding the thickness of the sensor, which is essential for analysis purposes. Although the sensor's specifications offer a value, our "calibration" process can detect any variations from the sensor's original thickness. By calibrating every experiment, we are able to identify and monitor any deviation.

$$f_n = \frac{n}{2h_q\sqrt{\frac{\mu_q}{\rho_q}}}$$ **Equation 31**

This equation is solved with h_q as unknow so the predicted values for f in each overtone are consistent with the experimental values.

5.5 Sample deposition

After verifying that the sensor is in optimal working condition, we can think about the best method to deposit the sample on the sensor surface according to the experiment. The main methods employed for sample deposition on QCM-D sensors include: flow deposition, drop casting, spin-coating, and spray-coating[4]. For the three last methods, a measure on air is done, then the sensor is taken out of the QCM-D chamber and the sample is deposited[4].

5.5.1 Drop casting

Drop casting consists of depositing the sample on the quartz sensor surface and allowing it to evaporate, leaving behind a thin film[4]. Usually, the obtained film is heterogeneous, as in the coffee ring effect, and it has some reproducibility issues.

We chose this method to analyze the soft films. Which involves coating the sensor with diluted meibum in chloroform, depending on the experiment from both healthy individuals or patients suffering from meibomian gland disease.

5.5.2 Spin-coating process

In the spin-coating process, a polymer solution is also applied over the sensor, yet it is rapidly rotated to ensure uniform distribution of the solution over the surface[50]. As the solution distributes all over the sensor, the solvent undergoes evaporation, resulting in the formation of a uniform and thin polymer layer[4]. Spin-coating offers the advantage of producing a consistently even and thin layer that is ideal for QCM-D[4]. This was the method used for the masurements of polydimethylsyloxane (PDMS) thin films. The base formulation of PDMS elastomer (Sylgard 184, Dow corning) was disolved in toluene (5% v/v) and shaken for 12 hours[5]. One part of the curing agent was added to 20 parts of PDMS solution to 100 µl of the mixture was spin coated at 5000 rpm for 30s on each sensor[5]. The PDMS was crosslinked at 60°C overnight and cooled before measuring its frequency and dissipation[5].

5.5.3 Spray-coating

Spray-coating is the process of converting a solution into aerosol, typically using an airbrush, and applying it to the sensor's surface[4]. The solvent then evaporates, leaving behind a uniform and thin polymer film. Care must be taken when using these procedures, as certain residues may accumulate at the rear of the sensor. Therefore, thorough cleaning is crucial[4].

5.5.4 Flow deposition

Flow deposition implies the sensor being immersed in a liquid, usually water or some buffer water based. When measuring a liquid or a solution that needs a reference liquid, is a good practice to begin with a stable baseline in air, as is easier to later have a stable baseline in liquid (Figure 12), also reference measurement in the same liquid is always required to distinguish the bulk liquid contribution from the film properties since QCM is sensitive to the bulk liquid's characteristics. For flow deposition a clean quartz crystal sensor is used to record a stable frequency and dissipation baseline on air, then the chamber is filled with

water or buffer and allowed to reach a steady baseline, next the tubbing is switched to the sample. Finally, water or buffer is reintroduced to wash out the excess off and measure the adsorbed sample. We employed this technique to apply thin polyethylemine (PE) coating on the gold sensor to analyze its viscoelastic properties (Figure 13).

It does not matter which method is chosen, but the film to be analyzed should be uniformly distributed and smooth in order to analyze it.

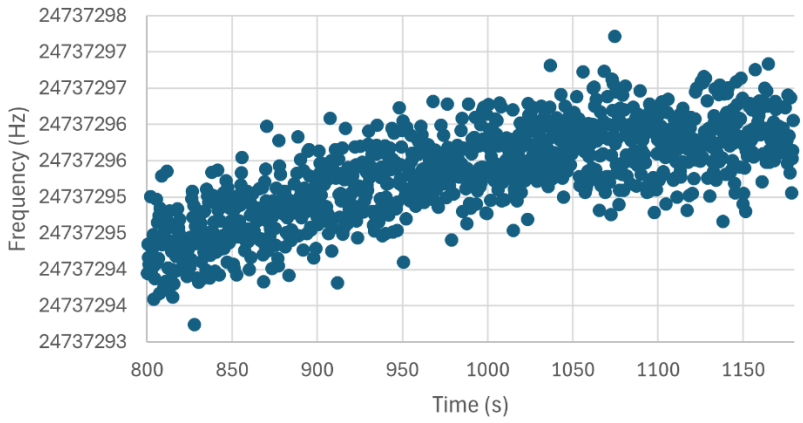

Figure 13. A stable PBS baseline.

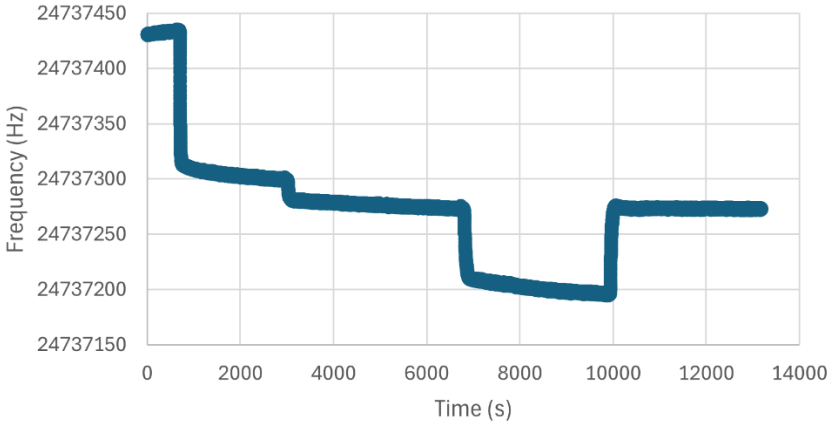

Figure 14. A typical flow deposition experiment. For this experiment we use the polymer Polyethylenimine (PEI) at different concentrations(3, 7 and 20 mg/ml) with a last step of PBS entrance to remove the excess.

5.6 Data analysis

It may appear straightforward to choose either Sauerbrey or Kanazawa-Gordon, when studying a solid or liquid material respectively. Yet there are certain materials that have both elastic and viscous components, depending on the amount and duration of applied shear stress, viscoelastic materials can exhibit either a primarily viscous or a mainly elastic, or equal, behavior. Is noteworthy to remember that QCMs work at really high frequencies, in the order of MHz and the rheological properties of some materials may change[6]. As dissipation is related to the viscous component, looking at dissipation raw data while doing the experiments, can be a first good approximation in the election of the analysis method[6,7]. Every experiment starts with the baseline, that could either be water or air, where frequency and dissipation values are ~ 0. When the sensor is loaded with a viscoelastic material, the frequencies decrease and spread at various overtones, and the dissipation values increase and spread at various overtones (Figure 14).

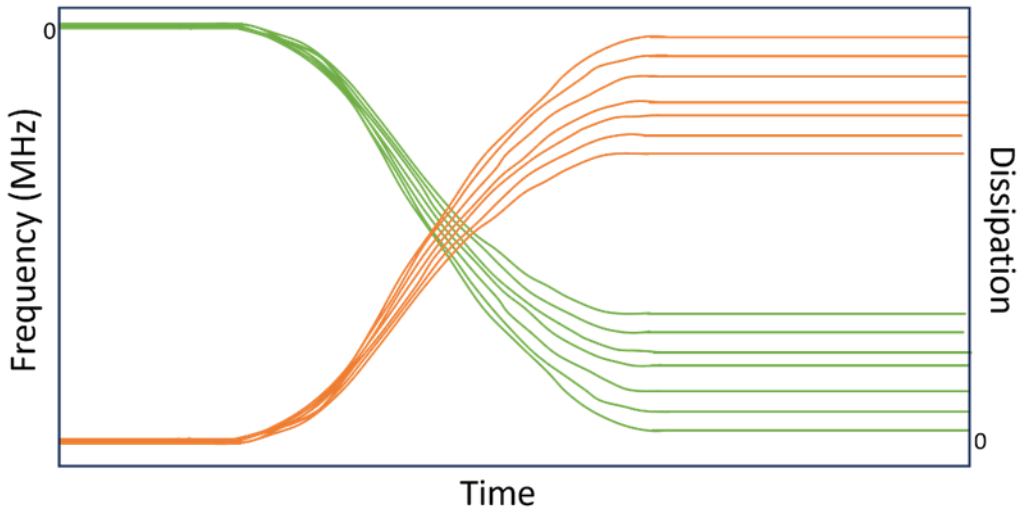

Figure 15. Scheme of a QCM-D experiment. Frequency is shown in green and dissipation in orange[8].

For data analysis we first have to extract our data, as we explain before, from sensor measured in air, in liquid (if is the case) for reference and with sample.To achieve optimal outcomes, it is advisable to utilize harmonics with values of n = 3, 5, and 7 for the purpose of modeling. It is important to be careful when using higher order harmonics because the interaction between anharmonic resonances and the main resonance peak can result in inaccurate measurements of Δf and ΔΓ[9]. Using a model with n = 1 is not recommended because non effective energy trapping[9].

We will be deriving a general equation that can be utilized for a viscoelastic layer in air, a semi-infinite viscoelastic fluid, a rigid layer in air and for a thin viscous film. There are two explanations in the literature for the change in frequency caused by a viscoelastic layer in a liquid. Although the language may vary, they are essentially the same. We know that for a thin viscoelastic layer immersed in a semi-infinite viscoelastic fluid layer[10]:

At the resonance frequency, the sound wave manifests as a standing wave, and the quartz sensor experiences a displacement (u_q). It is assumed that, owing to the unconstrained nature of the plate's surfaces, the stress (σq) at both surfaces (z = 0 and z = hq) is zero. Furthermore, in the linear domain, stress is exactly

proportional to strain (εq), and it is also asserted that, within this regime, stress correlates with strain. What we are looking for is the stress-displacement ratio that for a quartz crystal sensor is:

$$\frac{\sigma_q}{u_q} = -\mu_q k_q \frac{\sin(k_q z)}{\cos(k_q z)} = -\mu_q k_q \tan(k_q z) \qquad \textbf{Equation 32}$$

Where K_q is the angular wavenumber.

A uniform thin film of viscoelastic material with thickness h_f covering the quartz sensor's top results in a shift in the resonance wavelength to adjust for the new unbound surface of the film, hence raising the stress on the sensor surface. The alteration in wavelength signifies a reduction in frequency (ΔF).The stress in the film, as a viscoelastic material, is out of phase with the strain by an angle θ. The stress-displacement ratio of the film is as follows:

$$\frac{\sigma_f}{u_f} = -{G_f}^* k_f \tan(k_f z) \qquad \textbf{Equation 33}$$

Under the assumption of a non-slip state, the stress-displacement ratio of the quartz and the film is equivalent at the surface (z=hq for the quartz, z=-hf for the film). We get the fundamental equation for a thin layer in air.

$$\tan\left(\frac{\pi \Delta F^*}{{F_0}^*}\right) = \frac{\sqrt{\rho_f {G_f}^*}}{2{F_0}^* h_q \rho_q} \tan\left(-2\pi h_f F^* \sqrt{\frac{\rho_f}{{G_f}^*}}\right) \qquad \textbf{Equation 34}$$

Typically, the argument of the tangent function on the left side of Eq. 34 is a minimal value (ΔF* is generally a few hundred Hz, whereas F_0* is in the GHz range).

$$\Delta F^* = \frac{\sqrt{\rho_f {G_f}^*}}{2\pi h_q \rho_q} \tan\left(-2\pi h_f F^* \sqrt{\frac{\rho_f}{{G_f}^*}}\right) \qquad \textbf{Equation 35}$$

Assuming that the real component of the complex frequency significantly exceeds the imaginary component (usually MHz compared to a few hundred Hz), and extending the complex modulus in the tangent function:

$$\Delta F^* = \frac{\sqrt{\rho_f G_f{}^*}}{2\pi h_q \rho_q} \tan\left[-\frac{\pi h_f F \sqrt{2\rho_f}}{\|G_f\|}\left(\sqrt{\|G_f\| + G_f{}'} + i\sqrt{\|G_f\| - G_f{}'}\right)\right] \quad \textbf{Equation 36}$$

5.6.1 Importance of film thickness

We must be really careful with the thickness used for our experiments, for first time users of QCM, determining the correct thickness for a material may be difficult because it is not immediately obvious, as it depends on the viscoelastic moduli, density and angular frequency. A common outcome of this phenomenon is that users frequently try to fit data for films that are thin and where the QCM is not responsive to viscoelastic properties. In the work of Shull and coworkers work, we can distinguish five regimes, the Sauerbrey, viscoelastic, film resonance, bulk like and overdamped[6,9]. The Sauerbrey regime applies to films that are thin enough, the mass is determined using the Sauerbrey equation, but there is insufficient data to accurately measure the rheological properties of the film. The viscoelastic regime is the desired one to use the QCM as a high-frequency rheometer. In the bulk regime, when the films are sufficiently thick, that is greater than the decay length of the shear wave[6,9]. The shear wave produced by the QCM propagates through the sample without reflecting off any barriers, allowing us to study the properties of the material in its bulk[6,9]. In this regime no mass information can be collected. Nevertheless, in this particular area, the viscoelastic characteristics are accurately ascertained by employing the combination of Δf and ΔΓ[6,9]. In the overdamped regime, the value of $\Delta\Gamma_n$ is so large that it prevents the formation of a distinct crystal resonance, there is a loss of signal of the overtones bigger overtones and the overtones that can be measured have a noisy signal[6,9]. Under this environment, a QCM experiment is incapable of providing any information[6,9]. Within the resonance regime, the reflected wave effectively enhances the crystal frequency by coupling with the propagating wave[6,9]. The viscoelastic characteristics calculated in this experiment will not yield significant data[6,9].

Since the real component (ΔF) in Equation 36 must be negative, the argument of the tangent function must lie within the interval of 0 to -π/2; thus:

$$\frac{\pi h_f F\sqrt{2\rho_f}}{\|G_f\|}\left(\sqrt{\|G_f\| + G_f{}'}\right) < \frac{\pi}{2}$$

$$h_f < \frac{\|G_f\|}{2F\sqrt{2\rho_f(\|G_f\| + G_f{}')}} \qquad \textbf{Equation 37}$$

Equation 37 defines the required film thickness to exclude resonance within the film. When the imaginary component of the tangent surpasses π, the tangent assumes the value of i; so, under this condition:

$$\frac{\pi h_f F\sqrt{2\rho_f}}{\|G_f\|}\left(\sqrt{\|G_f\| - G_f{}'}\right) > \pi$$

$$h_f > \frac{\|G_f\|}{F\sqrt{2\rho_f(\|G_f\| - G_f{}')}} \qquad \textbf{Equation 38}$$

Equation 38 establishes the requisite film thickness for obtaining saturation (semi-infinite film thickness).

We can also employ the method proposed by Shull and coworkers, the regimes beside Sauerbrey are deviations that can be explained by the ratio $\frac{h_1}{\lambda_n}$, where h_1 represents the film thickness and λ_n represents the shear wavelength of the mechanical oscillation in the medium at the nth overtone or harmonic.

$$\frac{h_1}{\lambda_n} = h_1 n f_0 \left(\frac{\rho_1}{G_1^*}\right)^{\frac{1}{2}} \qquad \textbf{Equation 39}$$

A Sauerbrey regime can be considered up to $\frac{h_1}{\lambda_n} \approx 0.05$, when viscoelastic films are thick enough, the ratio of $\frac{h_1}{\lambda_n}$ may reach 0.25, causing the frequency to increase as the mass increases. This goes against the expected trend described by the Sauerbrey statement. The film resonance effect also results in a substantial augmentation in Γ (or D), rendering the parameter challenging to measure with precision. The phenomenon of film resonance is most noticeable when $\frac{h_1}{\lambda_n} \approx 0.25$[9].

Hence, the domain in which viscoelastic properties may be precisely measured should fall within the range of $\frac{h_1}{\lambda_n} \approx 0.05 - 0.20$.

5.7 References

1. Edvardsson, M. (2010, December 8). Q-Sense E1 Operator Manual Including the acquisition software QSoft 401 . Sweden; Q-Sense.
2. (2008, March) Cleaning & Immobilization Protocols. Sweden; Q-Sense.
3. *QCM-D Tips and tricks – three steps to optimize the data quality* (no date) *Biolin Scientific*. Available at: https://www.biolinscientific.com/blog/qcm-d-measurement-tips-and-tricks-how-to-optimize-the-data-quality (Accessed: 06 February 2024)
4. Easley, A.D. *et al.* (2021) 'A practical guide to quartz crystal microbalance with dissipation monitoring of thin polymer films', *Journal of Polymer Science*, 60(7), pp. 1090–1.
5. M. Bracic, T. Mohan, R. Kargl, T. Griesser, S. Hribernik, S. Köstler, K. Stana-Kleinschek, and L. Fras-Zemljic, "Preparation of pdms ultrathin films and patterned surface modification with cellulose," RSC Advances 4, 11955–11961 (2014).
6. DeNolf, G. C., Haack, L., Holubka, J., Straccia, A., Blohowiak, K., Broadbent, C., & Shull, K. R. (2011). High frequency rheometry of viscoelastic coatings with the Quartz Crystal Microbalance. *Langmuir*, *27*(16), 9873–9879.
7. Reviakine, I., Johannsmann, D. and Richter, R.P. (2011) 'Hearing what you cannot see and visualizing what you hear: Interpreting quartz crystal microbalance data from solvated interfaces', *Analytical Chemistry*, 83(23), pp. 8838–8848.
8. Adaptado de: " Single-harmonic vs multi-harmonic QCM-D – what is the difference?" , por Malin Edvardsson, 2024, Biolin Scientific (https://www.biolinscientific.com/blog/single-harmonic-vs-multi-harmonic-qcm-d-what-is-the-difference).
9. Sadman, K., Wiener, C. G., Weiss, R. A., White, C. C., Shull, K. R., & Vogt, B. D. (2018). Quantitative rheometry of thin soft materials using the quartz crystal microbalance with dissipation. Analytical Chemistry, 90(6), 4079–4088.
10. Voinova, M. V., Rodahl, M., Jonson, M., & Kasemo, B. (1999, May 1). Viscoelastic Acoustic Response of Layered Polymer Films at Fluid-Solid Interfaces: Continuum Mechanics Approach. *Physica Scripta*, *59*(5), 391–396.

6.Viscoelastic analysis of the lipid layer: Influence of the lipid layer on the development of evaporative dry eye.

6.1 Introduction

The ocular surface is a vital component of vision[1]. Its function is to maintain the cornea's optical clarity by regulating the hydration of the cornea and conjunctiva, as well as protecting the eyeball from mechanical damage or infection[1]. It's a complicated structure that depends on many tissues working together properly[1,2]. For example, the layer of cells that covers the eye's surface (corneal epithelium, limbus, and conjunctiva), the edge of the eyelid, and the tear film are all important to this structure[1,2]. The tear film is an extremely varied colloidal biological system whose components are of glandular and cellular origin[2,3]. It consists of three non-well-defined layers: the mucous layer, constituted by mucins secreted by goblet and epithelial cells (figure 16). The lacrimal gland secretes the aqueous layer, while the meibomian gland secretes the lipid layer that covers its external surface[1,4]. Its main functions include nutrient distribution, corneal oxygenation control, and physical and antimicrobial protection[4].

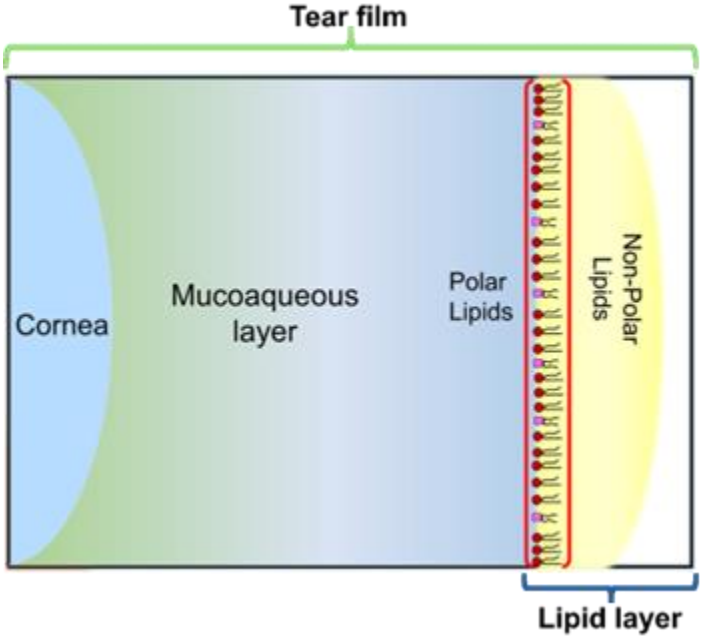

Figure 16.*Schematic representation of the most accepted view on the structure of the tear film. Polar lipids lay down above the mucoaqueous layer as a thin film with a relatively thick layer of nonpolar lipids above it.*

The lipid layer is the outermost layer of the tear film, which is exposed to the environment. It is composed of lipids from the meibomian gland[5]. This lipid secretion is known as meibum[5]. Individual meibomian glands express it to the ocular surface through a system of small ducts and a central duct, which terminates in an orifice at the margin of the eyelid[5]. Human meibum consists, in major proportion, of ~30-45 mol% of cholesteryl esters and ~30-50 mol% of waxy esters[6]. The major amphiphilic molecules secreted by the meibomian glands are (O-acyl) ω-hydroxy fatty acids (OAHFAs) these comprise ~2% of meibomian lipids[6]. Furthermore, minor quantities of triacylglycerides (~2%), free cholesterol (0.5%), and phospholipids (<0.01%) are also present[6]. The lipid layer, despite its name, is not only comprised of lipids. It also consists of around 22 wt% of non-lipid components, including proteins, salts, and polysaccharides[7,8]. Proteins and glycoproteins, including lipocalins, lysozyme, and mucin, are thought to be inserted into the lipid layer and improve its stability[7,8]. The lipid layer of the tear film is estimated to be between 15 and 160 nm thick[7,9-11]. Where meibomian lipids do not

spread as monolayers at the air/water interface but form thick duplex films[7,9-11]. The most accepted view assumes that polar lipids form the lower sublayer, i.e., the interface between the lipid layer and the aqueous layer, and non-polar lipids form the upper part, which is in contact with the air[7,9-11]. The lower sublayer creates an interface that helps stabilize the upper portion[10]. In addition, the formation of hydrophobic lipid clusters in lenses under high surface pressures is proposed[6]. The formation of these lenses could be critical to allow diffusion of the lipid layer after blinking[6]. By spreading over the water phase, the lipid layer lowers free energy, making the tear film more stable, thickens the water phase through the Marangoni effect, and slows down evaporation[3]. An increased evaporation rate is related to evaporative dry eye syndrome. Dry eye syndrome has a great impact on visual function of people suffering it from, affecting its quality of life, due to symptoms like: burning or feeling of pressure in the eyes, sensation of sand or foreign body, tearing, pain that may be localized somewhere in the eye, behind the eye or even around the orbit; redness is a common complaint, intermittent blurred vision that may also be described as halos around lights at night, feeling of heaviness in the eyelids or difficulty opening the eyes, dryness and tired eyes[12,13]. Our group observed through microevaporation experiments, that meibomian lipid films significantly decrease the evaporation rate and that the evaporation with meibomian lipids from diagnosed patients is higher than lipids from healthy patients[14,15].

Meibomian lipids provide a smooth optical surface for the cornea, act as a barrier against foreign particles, have antimicrobial activity, and seal the lid margins during prolonged closure[3]. As a result, the lipid layer plays a vital role in maintaining the homeostasis of the ocular surface[3]. Problems with its stability and breakdown can cause dry eye symptoms[3]. The predominant cause of this type of dry eye disease is meibomian gland dysfunction (MGD), due to changes in meibum composition leading to variations in melting and spreading properties of meibum. Its stability is crucial to withstand a range of different stresses and deformations, with viscoelasticity being the main characteristic that allows it to resist deformation[16].

Meibomian lipids are the primary component of the lipid layer; therefore, the physical properties of these materials could be critical for the tear film's functionality[17]. Studying reological properties is crucial, as they rely on the compression and expansion forces produced by the eyeball or eyelid movements, as well as the speeds and amplitudes at which these movements occur[18]. Because the lipid layer experiences distinct types of deformation, it cannot be characterized by a single technique[19]. Very few studies have been conducted on the bulk rheology of the human meibum[20,21]. Tiffany and Dart measured viscosity values for the human meibum using a capillary tube and estimated values from 9.7 to 19.5 Pa·s at 35°C[20,21]. These studies were semi-quantitative and did not explore the role of the shear rate or temperature[20,21]. Later, Yokoi et al. demonstrated that time-dependent changes in the propagation of the tear film's lipid layer are consistent with the Voigt reological model, suggesting that the lacrimal film has viscoelastic properties, and concluded that the lipid layer is elastic and drags up to the underlying tear film[20,22]. In 2013, Rosenfeld et al. found that bulk meibum is both viscous and elastic; at 35 °C, the shear viscosity of bovine and human meibum is approximately 105 greater than that of water, and it has high shear fluidization even at temperatures as high as 150 °C, indicating that the meibum is structured and inhomogeneous[20]. Both bovine and human meibum exhibit strong elasticity, with an elastic modulus greater than the viscous modulus[20]. The values of the elastic modulus range from around 102 to 103 Pa at a temperature of 35 °C and a frequency of 1 Hz[20]. The results of oscillatory rheology studies indicate that meibum exhibits mostly elastic behavior up to a temperature of 140 °C[20]. Within the temperature range of 30 to 36 °C, both stationary and oscillatory rheology demonstrated a significant decrease in the viscosity of meibum, as well as in the elastic and viscous moduli[20]. This indicates the presence of crystalline material that undergoes melting at temperatures exceeding the specified range[20]. Leiske et al. examined the viscoelasticity of human and animal meibomian lipids under shear-type deformation using a magnetic needle rheometer in a frequency sweep[17]. The interfacial viscoelastic properties of lipid samples obtained from humans, cattle, koalas, wallabies, and rabbits exhibited the same behavior[17]. At surface pressures

ranging from 5 to 10 mN/m, the material showed elastic behavior, with a viscous modulus of zero and an elastic modulus that rose in a linear manner with frequency[17]. At a surface pressure of 15 mN/m, both viscous and elastic moduli increased, with elastic behavior dominating[17]. At 20 mN/m, the elastic and viscous moduli remained invariant with frequency, which is a characteristic behavior of a gel[17]. In a subsequent study, the same research group considered the effects of temperature on lipids[23]. This is important because of the transition temperature of meibomian lipids. Shear-type deformations were applied, and it was shown that, as the temperature increased, the viscoelastic modulus decreased[23].The elastic modulus dominated the lipid films until 20 °C, at which point the viscous modulus took over[23]. The elastic modulus dropped to an unrecordable level above 30 °C[23]. Meibomian lipids have also been subjected to dilatational deformations, to emulate lipid film compression and expansion[16]. Svitova et al, used the sessile bubble configuration to investigate the interfacial dilatational rheological properties of thick films of lipids extracted from contact lenses[3]. The lipid films exhibited viscoelastic behaviors when subjected to small and uniform radially dilated deformations[3]. In addition, they examined how the interaction of lipids with the model tear protein, lysozyme, affects the mechanical properties, showing that the interfacial rheological characteristics of lipid films are altered by interactions with lysozyme[3,24]. Raju et al. (2013) investigated the viscoelastic characteristics of meibomian lipid films under dilatational deformations using the pendant drop method[16]. Experiments were performed at room temperature and physiological temperature, and the effects of altering the composition of the lipid films with tiny amounts of cholesterol and β-carotene were also analyzed[16]. At both 37 and 20 °C, the elastic modulus (E') was more dominant than the viscous modulus (E''), indicating that the lipid films were more solid than fluid, despite temperature[16]. E' and E'' were frequency-dependent, indicating molecular rearrangements during expansions and compressions. Modified lipid films exhibited a slight increase in moduli[16]. Georgiev et al. investigated the surface dilatational rheology of meibomian lipid samples, obtained from both healthy eyes and eyes with meibomian gland dysfunction[25]. They employed a Langmuir trough and the

deformation-relaxation method for their analysis[25]. The surface pressure was measured during these studies after a small and fast compression was applied25. Viscoelastic properties of samples from ill patients exhibited both similarities and differences compared to samples from healthy people[25]. Both types were predominantly elastic at high frequencies (>2.5 X 10^{-2} Hz), however in the 10^{-4} to 10^{-3} Hz range, lipids from diseased patients became predominantly viscous, while healthy lipids maintained their elastic properties[25]. The objective of this work was to study the rheological properties of meibomian lipids from healthy persons and patients with some dysfunction of the meibomian glands through QCM-D at different temperatures.

6.2 Materials and methods

6.2.1 Meibum collection

The subjects recruited underwent diagnostic tests to assess ocular surface status, including 1) OSDI quality of life test, 2) tear film breakup time TRPL, 3) Schirmer's test, 4) ocular staining, 5) tear meniscus evaluation, 6) analysis of palpebral morphology and meibomian gland secretion. The case group consists of patients with meibomian gland dysfunction, following the International Workshop on Meibomian Gland Dysfunction (IWMGD) classification, with clinical data including palpebral margin abnormalities, meibomian gland outflow orifice obstruction and poor quality of secretion, in addition to clinical symptoms such as pruritus, ocular discomfort, lacrimation and photophobia. Subjects with any previous ocular or systemic pathology, subjects with a history of active ocular infection, allergic conjunctivitis, autoimmune diseases, contact lens wearers, history of topical medication use, glaucoma and previous ocular surgery were excluded. Pregnant or lactating women were also excluded. Control subjects were healthy individuals with no history of ocular surgery or pathology and no history of topical ophthalmologic medication use. The protocol described here was carried out with the tenets of the the Declaration of Helsinki, approved by the ethics committee of the Instituto de oftalmología Fundación Conde de Valenciana, and was performed with the

informed consent of all participants. The 4 eyelids of each individual were pressed using a cotton swab which resulted in the extrusion of meibomian lipids through the orifices of the meibomian glands, the secretion was removed by passing a platinum spatula. Approximately 1 mg of lipid secretion was collected per individual, which was immediately transferred to a vial with 1 ml of chloroform. The vials were stored at -80 °C for preservation.

6.2.2 QCM-D Measurements

After cleaning and calibration procedures described previously, experiments were performed by measuring frequency and dissipation shifts of meibum coated sensors using a Quartz Crystal Microbalance with Dissipation (Q-Sense E1, Biolin Scientific). A clean blank quartz crystal sensor was used to record a frequency and dissipation stable baseline on air, after that measurement the sensor was coated depending on the experiment with meibum from both healthy individuals and patients suffering from meibomian gland diseases by drop casting and then loaded into the QCM-D to determine meibum mass and layer thickness at 25°C using Saurbrey equation. Lastly, a temperature ramp was programmed with temperatures ranging from 25 to 42°C, frequency and dissipation data from multiple overtones were analyzed by the SLA model to obtain the storage moduli and the loss moduli.

6.3 Results and discussion

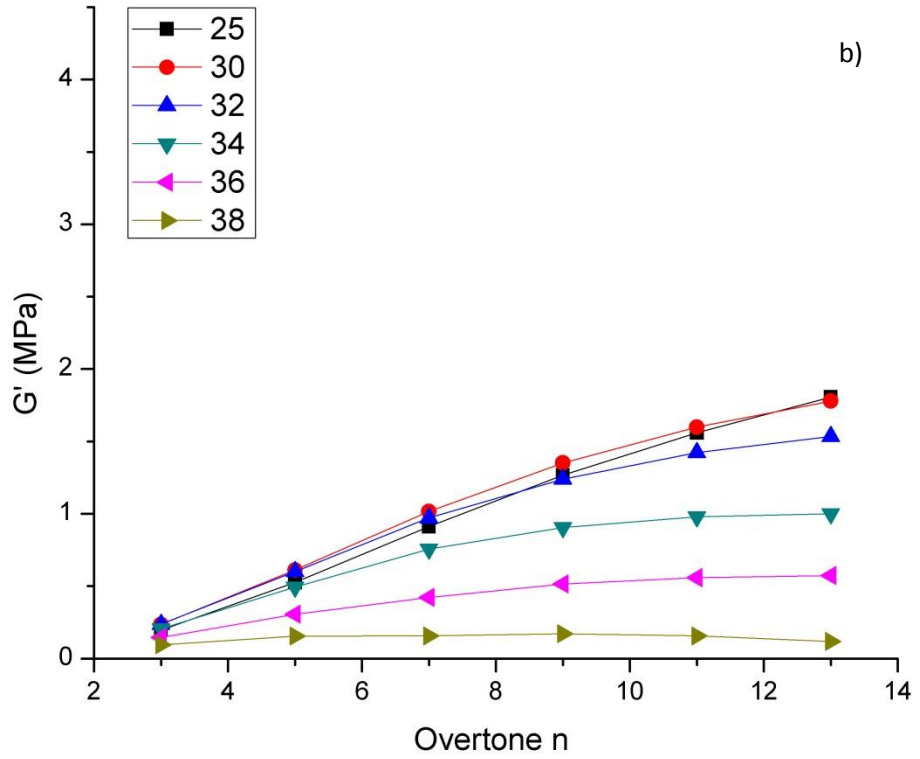

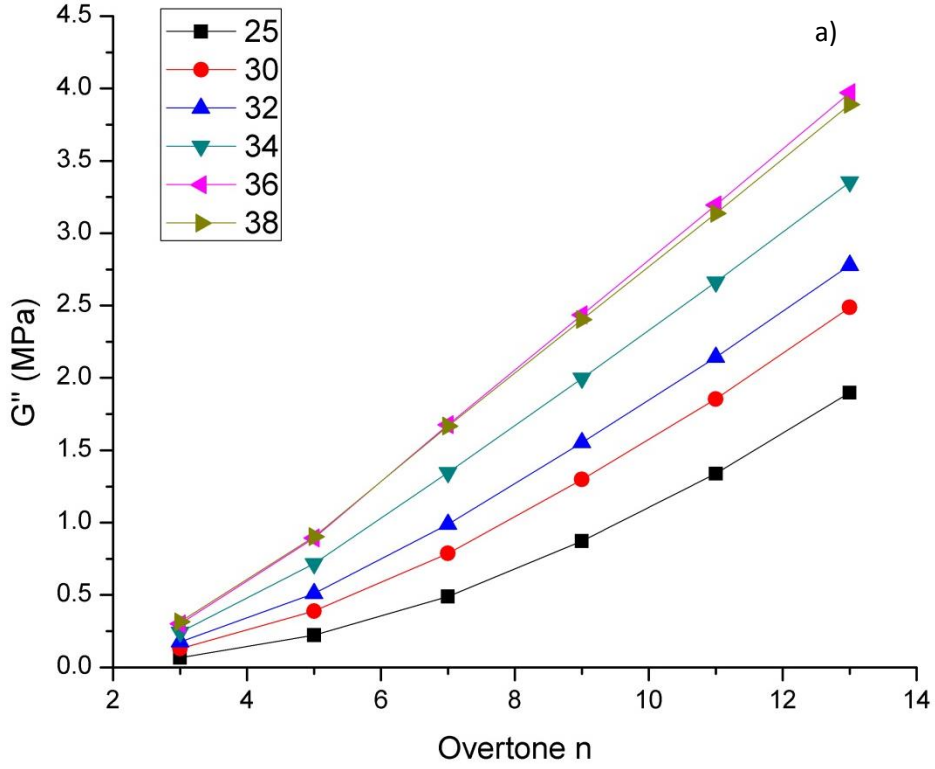

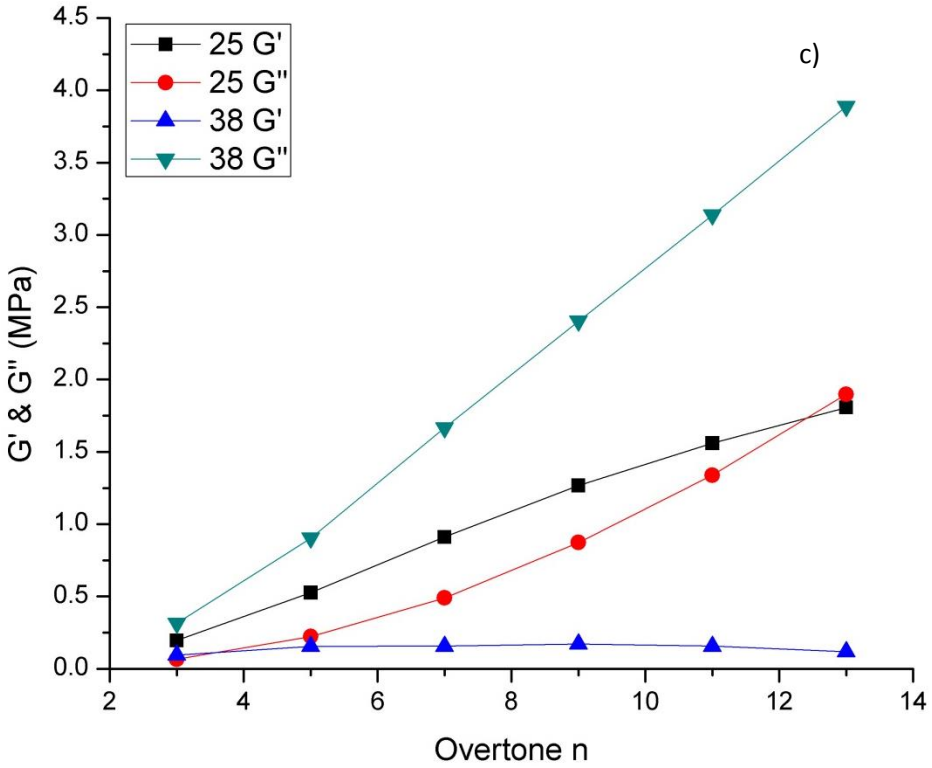

Figure 17. Bulk moduli as a function of temperature for a representative human meibum *sample from a healthy volunteer.* Measured at various frequencies ranging from 5 MHz to up to 65 MHz. The film was kept at room temperature initially and then heated it up to 38°C. In a) The elastic modulus is shown G' at different temperatures. In b) The viscous modulus G'' is shown at diferent temperatures. In c) there is a comparasion between G' and G'' at 25°C and G' and G'' at 38°C.

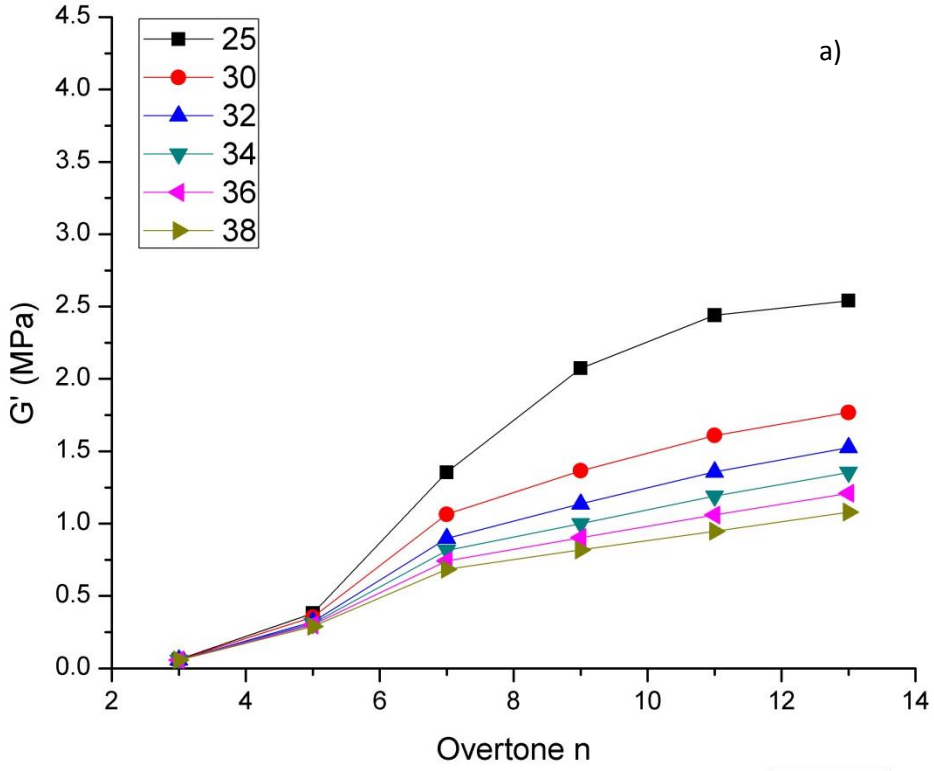
a)
25
30
32
34
36
38
G' (MPa)
Overtone n
0.0
0.5
1.0
1.5
2.0
2.5
3.0
3.5
4.0
4.5
2
4
6
8
10
12
14

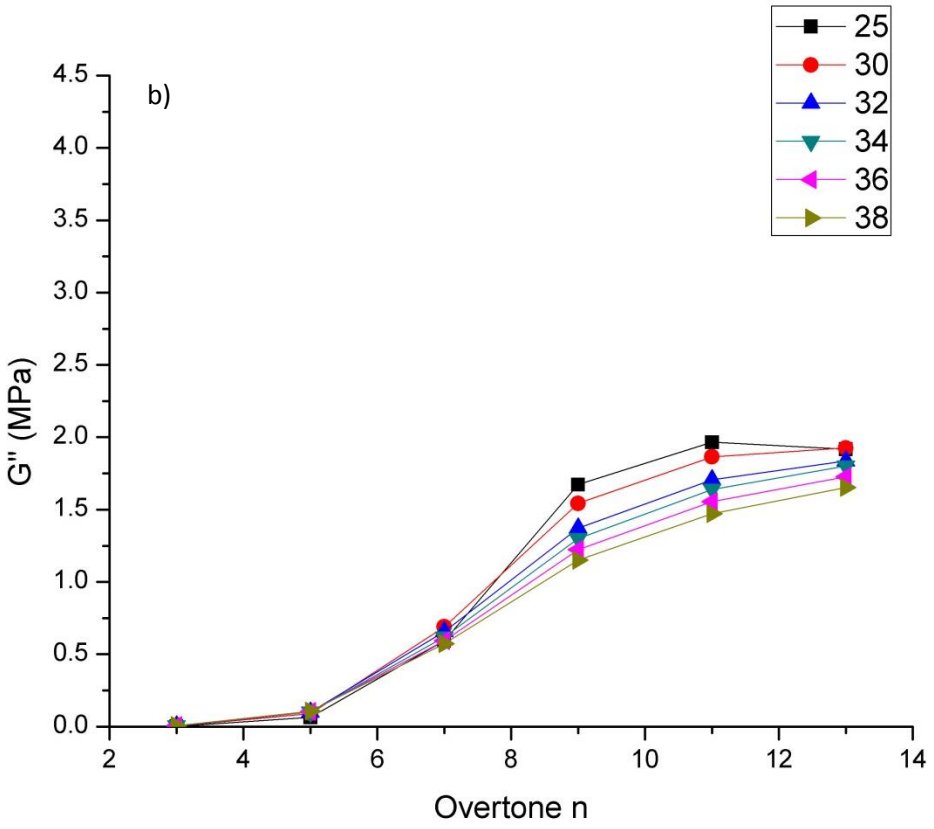
b)
25
30
32
34
36
38
G'' (MPa)
Overtone n
0.0
0.5
1.0
1.5
2.0
2.5
3.0
3.5
4.0
4.5
2
4
6
8
10
12
14

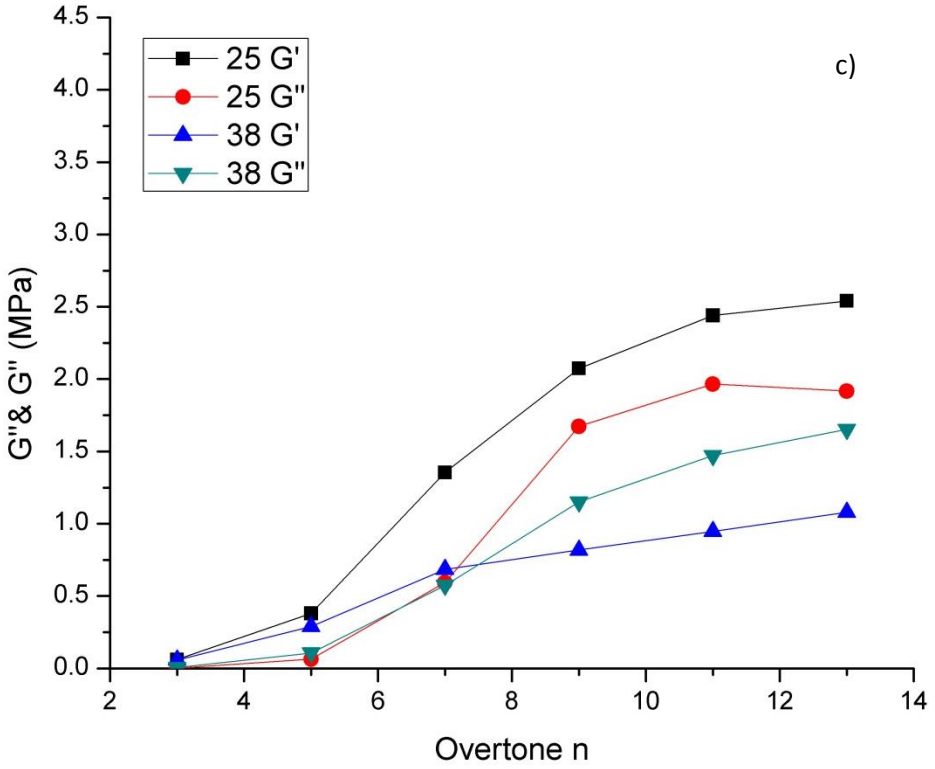

Figure 18. Bulk moduli as a function of temperature for a representative human meibum sample from a pacient with dry eye disease. Measured at various frequencies ranging from 5 MHz to up to 65 MHz. The film was kept at room temperature initially and then heated It up to 38°. In a) The elastic modulus is shown G' at different temperatures. In b) The viscous modulus G'' is shown at diferent temperatures. In c) there is a comparasion between G' and G'' at 25°C and G' and G'' at 38°C. The frequency at each overtone is the fundamental frequency times each overtone.

The viscoelastic properties obtained with the QCM-D of human meibum are presented in figure 17 for the healthy meibum and figure 18 for the diseased meibum. Temperature sweeps from 25 to 38C we're performed as presentedin figure 17 and 18. The findings corroborate that human meibomian lipids are a viscoelastic material. For the healthy meibum sample at 25C , G' was dominant over G''. At 25C lipids are more solid or rigid like, yet we still have the G' component, which makes sense as it is reported that meibomian lipids begin to soften ~19C. We tried to make experiments at 15C (data not shown) but it was difficult to regulate this temperature in the QCM-D, It will be interesting trying to replicate thoose experiments in orden to see how G' and G'' behave at low temperatures. Around 32C the later behaviour switched and G'' started to take over

which was somehow expected as meibomian gland lipids have a melting point around 29-33C. At the different temperatures, the moduli were dependant on frequency as there was an increase in the moduli with increasing frequency. As there was an increase in the moduli with increasing frequency. For the sample from the diseased meibum, we measured lower G' and G''. They doesn't change that much with temperature, and It is also Frequency dependant. Surprisingly few studies have been conducted on the bulk rheology of human meibum, despite its relevance to meibum behavior in the eye. One of the initial attempts was Tiffany and Dart's semiquantitative study, which failed to investigate the effects of shear rate or temperature. Meibum's ability to secrete from the glands onto the ocular surface is one of its fundamental characteristics. Temperature fluctuations influence this characteristic. In a healthy eye, at body temperature, meibum must possess a liquid-like consistency that enables it to traverse the meibomian gland ducts and exit through the gland orifices to ultimately spread lipids onto the tear film surface. Upon contact with the ocular surface, meibum lipids undergo cooling, leading to enhanced rigidity. The lipid layer is resposible for controlling evaporation of the tear film. Pathological conditions cause changes in the meibum's composition, which alter its texture and melting temperature, thereby complicating its expression. A reduced lipid supply would result in increased evaporation of the aqueous layer.

In a work by Rosenfeld et al. Bulk rheology of human and bovine meibum across various temperatures, oscillation frequencies, and shear rates was investigated. They found that bulk meibum exhibits both viscosity and elasticity. At 35°C, the shear viscosity of bovine and human meibum is roughly 10^5 times greater than that of water. Similarly, bulk meibum exhibits significant shear thinning properties even at temperatures reaching 150C. Bovine and human meibum exhibit significant elasticity, with elastic moduli surpassing their viscous moduli. The viscous and elastic moduli of bovine and human meibum are roughly 102 to 103 Pa at 35°C and 1 Hz. Oscillatory rheology indicates that meibum mostly exhibits elasticity up to 140°C. Both steady and oscillatory shear rheology exhibit a significant reduction in meibum viscosity and in the storage and loss moduli

between 30 and 36°C. Changes in the melting temperature has been reported by Borchman et al., they utilized infrared spectroscopy to illustrate that the meibum melting temperature in patients with meibomian gland dysfunction is elevated compared to control patients.One of the main differences betweeen our study and what is already on the literature, lay in the method use to asses the elastic and viscous moduli. We implemented the use of the QCM-D, as this technique allowed the use of a minimal quantity of sample and an individualized analysis, so we we're capable of measuring samples from single pacients and healthy people. When the usual is to measure mixed samples from several individuals on a tradicional rheometer. On the article by Rosenfeld et al. Experiments where carried out at a frequency of 1 Hz, whereas we conducted our experiments at a minimum of 5 MHz. We observe a shift in the modulus from a dominant elastic modulus to a dominant viscous modulus. While bovine meibum maintained its elasticity up to 140 C, the G' modulus dominates the G'' modulus in human meibum, and their similarities are striking. While our control sample experienced a significant reduction in G' at 32-34 degrees in every undertone, our case sample showed a similar G' and G'' modulus at lower overtones, with the G'' modulus taking over only at higher frequencies. This differences may be related to the technique used in both studies and to the cuantity of meibum used. For our experiments we used films of around 100 to 150 nm so we we're working somewhere beetween the bulk rheology and the interfacial rheology. The moduli were really sensitive to temperature. In pathological conditions, such as inflammation caused by dry eye or other visual disorders, slight variations in temperature may substantially affect the integrity of the lipid layer.

6.4 Conclusions

We were able to measure the rheology of individual meibomial lipid samples, when it is usual to measure mixed samples from several individuals. The clinical distinction between healthy and diseased conditions, such as dry eye or meibomian gland dysfunction (MGD), has been limited by the absence of objective assessments. The QCM-D could be an option to elucidate how viscous and elastic moduli change with temperature in healthy and diseased states. There still some

work to be done, as the samples utilized where old and diluted in chloroform, we are working in orden to get new and fresh samples. Also we need to work in the statistical analysis, as we end with to many measurements.

6.5 References

1. Tsubota K., Tseng S.C., Nordlund M.L. (2002) Anatomy and Physiology of the Ocular Surface. In: Ocular Surface Disease Medical and Surgical Management. Springer, New York, NY.

2. Yañez-Soto, B., Mannis, M. J., Schwab, I. R., Li, J. Y., Leonard, B. C., Abbott, N. L., & Murphy, C. J. (2014). Interfacial Phenomena and the Ocular Surface. The Ocular Surface,12(3), 178-201

3. Svitova, T. F., & Lin, M. C. (2016). Dynamic interfacial properties of human tear lipid films and their interactions with model-tear proteins in vitro. Advances in Colloid and Interface Science,233, 4-24.

4. Dilly P.N. (1994) Structure and Function of the Tear Film. In: Sullivan D.A. (eds) Lacrimal Gland, Tear Film, and Dry Eye Syndromes. Advances in Experimental Medicine and Biology, vol 350. Springer, Boston, MA.

5. Butovich, I. A. (2017). Meibomian glands, meibum, and meibogenesis. Experimental Eye Research,163, 2-16.

6. Millar, T. J., & Schuett, B. S. (2015). The real reason for having a meibomian lipid layer covering the outer surface of the tear film – A review. Experimental Eye Research,137, 125-138.

7. Georgiev, G. A., Eftimov, P., & Yokoi, N. (2017). Structure-function relationship of tear film lipid layer: A contemporary perspective. Experimental Eye Research,163,17-28.

8. Bron, A. J., Tomlinson, A., Foulks, G. N., Pepose, J. S., Baudouin, C., Geerling, G., . . . Lemp, M. A. (2014). Rethinking Dry Eye Disease: A Perspective on Clinical Implications. The Ocular Surface,12(2).

9. King-Smith, P. E., Hinel, E. A., & Nichols, J. J. (2010). Application of a Novel Interferometric Method to Investigate the Relation between Lipid Layer Thickness and Tear Film Thinning. Investigative Opthalmology & Visual Science,51(5).

10. Green-Church, K. B., Butovich, I., Willcox, M., Borchman, D., Paulsen, F., Barabino, S., & Glasgow, B. J. (2011). The International Workshop on Meibomian Gland Dysfunction: Report of the Subcommittee on Tear Film Lipids and Lipid–Protein Interactions in Health and Disease. Investigative Opthalmology & Visual Science,52(4), 1979.

11. Cwiklik, L. (2016). Tear film lipid layer: A molecular level view. Biochimica Et Biophysica Acta (BBA) - Biomembranes,1858(10), 2421-2430.

12. Miljanović, B., Dana, R., Sullivan, D. A., & Schaumberg, D. A. (2007). Impact of dry eye syndrome on vision-related quality of life. American Journal of Ophthalmology, 143(3).

13. Golden MI, Meyer JJ, Patel BC. Dry Eye Syndrome. [Updated 2021 Nov 2]. In: StatPearls [Internet]. Treasure Island (FL): StatPearls Publishing; 2022 Jan- Available from: https://www.ncbi.nlm.nih.gov/books/NBK470411/

14. Blanco, D. C. (2018). Microevaporación no homogénea en modelos biofísicos (Tesis de maestría). Universidad Autónoma de San Luis Potosí.

15. Blanco-Campoy, D. G., Graue-Hernández, E. O., Quiróz-Casian, N., Vélez-Cordero, J. R., & Yáñez-Soto, B. (2022). In-vitro evaluation of the evaporation retardation by Meibomian lipids in homogeneous and non-homogeneous evaporation. Journal of Colloid and Interface Science, 625, 210–219.

16. Raju, S. R., Palaniappan, C. K., Ketelson, H. A., Davis, J. W., & Millar, T. J. (2013). Interfacial Dilatational Viscoelasticity of Human Meibomian Lipid Films. Current Eye Research,38(8), 817-824.

17. Leiske, D. L., Raju, S. R., Ketelson, H. A., Millar, T. J., & Fuller, G. G. (2010). The interfacial viscoelastic properties and structures of human and animal Meibomian lipids. Experimental Eye Research,90(5), 598-604.

18. Tiffany J.M. (1994) Viscoelastic Properties of Human Tears and Polymer Solutions. In: Sullivan D.A. (eds) Lacrimal Gland, Tear Film, and Dry Eye Syndromes. Advances in Experimental Medicine and Biology, vol 350. Springer, Boston, MA.

19. Adamson, A. W., & Gast, A. P. (1997). Physical chemistry of surfaces. New York: J. Wiley.

20. Rosenfeld, L., Cerretani, C., Leiske, D. L., Toney, M. F., Radke, C. J., & Fuller, G. G. (2013). Structural and Rheological Properties of Meibomian Lipid. Investigative Opthalmology & Visual Science,54(4), 2720.

21. Braun, R. J. (2012). Dynamics of the Tear Film. Annual Review of Fluid Mechanics,44(1), 267-297.

22. Yokoi, N., Yamada, H., Mizukusa, Y., Bron, A. J., Tiffany, J. M., Kato, T., & Kinoshita, S. (2008). Rheology of Tear Film Lipid Layer Spread in Normal and Aqueous Tear–Deficient Dry Eyes. Investigative Opthalmology & Visual Science,49(12), 5319.

23. Leiske, D. L., Leiske, C. I., Leiske, D. R., Toney, M. F., Senchyna, M., Ketelson, H. A., . . . Fuller, G. G. (2017). Temperature-Induced Transitions in the Structure and Interfacial Rheology of Human Meibum. Biophysical Journal,113(11), 2575.

24. Svitova, T. F., & Lin, M. C. (2013). Racial Variations in Interfacial Behavior of Lipids Extracted From Worn Soft Contact Lenses. Optometry and Vision Science,90(12), 1361-1369.

25. Georgiev, G. A., Yokoi, N., Ivanova, S., Tonchev, V., Nencheva, Y., & Krastev, R. (2014). Surface relaxations as a tool to distinguish the dynamic interfacial properties of films formed by normal and diseased meibomian lipids. Soft Matter,10(30), 5579-5588.

7.Appendix

7.1 Appendix 1

7.2 Introduction

Polymers intricately connect to various aspects of daily living and significantly influence individual quality of life[1]. Applications range from everyday plastics to sophisticated biopolymers found in medical equipment[2]. Key parts of studying and making new polymer-based materials are controlling how they build up, change shape, and break down[2]. The Quartz Crystal Microbalance with Dissipation monitoring, or QCM-D, has been used to characterize a number of polymers because it can track changes in the layers' mass and softness in real time[2,3]. However, because polymers typically have a viscous component, the modeling of the raw data can become complex[4]. The QCM-D can be utilized for the following purposes[3]:

- Polyelectrolyte Film Layer-by-Layer assembly monitoring.
- Thin polymer films thickness evaluation.
- Examine how the end-grafted polymer chains' conformation relates to the solvent environment.
- Examine how polymer layers react to changes in external factors such as pH, temperature, and salt concentration.
- Characterize molecular interactions with polymer layers, including binding, protein repellency, and antifouling capabilities.

In order to verify the applicability of the existing models for QCM-D data analysis, we studied the viscoelastic properties of Polydimethylsiloxane (PDMS) and Polyethyleneimine (PEI) adsorption. In the case of PMDS it is reported in literature that behaves as a kelvin voigt solid, and we verify that at really high frequency, it still behaves as a kelvin voigt solid. We used PEI as a model to

expand our knoledge in QCM-D data analysis. The most common model for QCM-D data analysis is the one attributed to Voinova, we utilized our algorithm to analyzed data, and realize that works better thanks using voinova's simplification.

PDMS is a transparent, non-toxic, viscoelastic silicon-based organic polymer characterized by hydrophobic surface chemistry[5,6,7]. Its remarkable optical, electrical, and mechanical qualities make it highly suitable for various applications[5,6,7]. PDMS has been utilized in micropumps, catheter surfaces, dressings and bandages, microvalves, optical systems, in vitro disease studies, implants, microfluidics, and photonics[7,8]. QCM-D has been employed to characterize PDMS interaction with biomolecules since PDMS exhibits a significant non-specific binding/interaction towards proteins, cells, and antibodies, which makes its native hydrophobic surface not optimal for applications such as cell growth, blood compatibility, and biomedical implants without appropriate surface modification, despite its benefits[7,8]. With a single QCM sensor and an adsorption layer made of metal-organic frameworks and PDMS, QCM-D has been utilized as a sensor for volatile organic compounds (VOCs)[9]. This makes it possible to detect and accurately identify a variety of VOCs under conditions of variable relative humidity[9]. We analyzed the viscoelastic properties of thin PDMS films with a thickness of around 150 nm. We found that they follow a kelvin voigt model. Understanding the rheological characteristics of PDMS is crucial for the effective functioning of all applications involving this material.

Polyethyleneimine (PEI) is a synthetic cationic polymer, either linear or branched, offered in a wide spectrum of molecular weights spanning from 700 Da to 1000 kDa[10]. Due to its composition of repeated ethylamine units, PEI exhibits significant water solubility[10]. It has antibacterial properties, PEI infiltrates and disrupts bacterial cell membranes, resulting in cellular death[11]. They serve as primary constituents for certain antimicrobial coatings used in medical devices and drug transporters within biomedical applications[10,11]. Moreover, PEI has been employed as a drug carrier in biomedical applications owing to its capacity to infiltrate cells or

permeabilize cell membranes[10,11]. Polyethyleneimine has been utilized in gene therapy, filtration technologies, and tissue engineering[10,11].

Given the favorable characteristics of PEI It has been applied to the layer-by-layer (LbL) technique for the construction of polyelectrolyte (PE) multilayers which has applications in industry and technology. The pulp and paper industry has created PEs from cellulose fibers and employed PEI and microfibrillated cellulose to construct multilayers for examination via QCM[12]. The primary objective has been to improve paper strength by sequentially treating a fiber solution with polyelectrolytes before sheet formation[12]. Another example, incorporating PEI into clay produces stable and dense layers in humid conditions, a significant advancement for the application of clay coatings[13].

The QCM-D technology, combined with a PEI coating, has functioned as a biosensor, such as a QCM-biosensor for the detection of Hepatitis B surface antigen (HBsAg)[14]. In summary, the surface modification of the gold electrode with PEI resulted in the covalent conjugation of anti-HBsAg antibodies to the primary amines[14]. QCM-D may be utilized to observe real-time damage to genomic mammalian DNA adsorbed on a PEI surface[15]. We quantified PEI adsorption utilizing PEI solutions at varying concentrations across two distinct pH levels: 7 and 12.

7.2 Materials and methods

7.2.1 Quartz Crystal Microbalance with Disipation (QCM-D) experiments with PDMS

Prior to utilization, 5 MHz quartz sensors coated with gold (QSX 301, Biolin Scientific) were immersed in a 5:1:1 H2O/H2O2/NH4OH solution at 75°C for ten minutes for cleansing, subsequently rinsed with deionized water, and dried using nitrogen gas. The frequency and dissipation changes of polydimethylsiloxane (PDMS) thin films were evaluated using a Quartz Crystal Microbalance with Dissipation (QSense E1, Biolin Scientific) to assess their viscoelastic properties. Only uncontaminated sensors were employed to document the constant frequency

and dissipation baselines. Subsequent to calibrating the sensors in air, they were extracted from the chamber for coating. The foundational formulation of PDMS elastomer (Sylgard 184, Dow Corning) was solubilized in toluene (5% v/v) and agitated for 12 hours. One part of the curing agent was included into 20 parts of the PDMS solution, and 100 µL of the resultant mixture was spin-coated at 5000 rpm for 30 seconds on each sensor. The PDMS was crosslinked at 60°C overnight and subsequently chilled prior to measuring its frequency and dissipation. The film thickness hf was determined by applying the Sauerbrey equation for n = 3 and 5, then extrapolating the value of Δf to n = 0. We utilized a density of $\rho f = 965\ kg/m^3$ in the relation $hf = mf/\rho f$.

7.2.2 Quartz Crystal Microbalance with Disipation (QCM-D) experiments using PEI

A Phosphate buffered saline tablet (Sigma-Aldrich, CAS:P4417) was diluted with 200 ml of deionized water to prepare PBS at pH 7.4. As PBS pH 12 was also used, pH was adjusted using a 0.1 M HCl solution. A 10 mg per ml PEI stock solution was prepared. The 50 wt% PEI solution (Sigma-Aldrich, CAS:9002-98-6) which has an average molecular weight of ~750,000 was diluted with diluted water. With the stock solution a 5,1,0.5, 0.1 mg per ml was prepared. Before every experiment, a 5MHz gold-covered sensor (QSX 301,Biolin Scientific) was cleaned on a 5:1:1 H2O/H2O2/NH4O mixture at 75°C for 10 minutes, rinsed thoroughly with deionized water and dried with nitrogen gas. The clean sensor was used to record a stable frequency and dissipation baseline on air, then the chamber was filled with PBS buffer at pH 7.4 and 12 depending on the experiment and allowed to reach a steady baseline. A concentration ramp was achieved by changing the tubbing from less concentrated PEI-PBS sample to the 10 mg per ml. Finally, buffer is reintroduced to watch out the excess and measure the adsorbed sample.

7.3 Results and Discussion

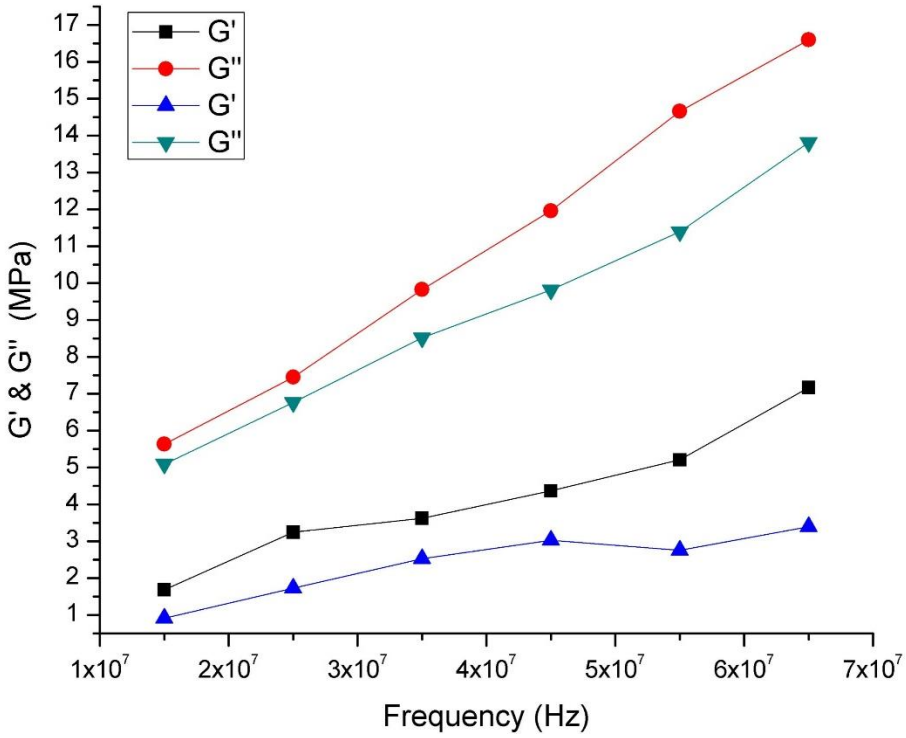

Figure 19. Elastic and viscous moduli of 150 nm PDMS films.Red and black symbols represent experiment one, and green and blue epresent experiment two.

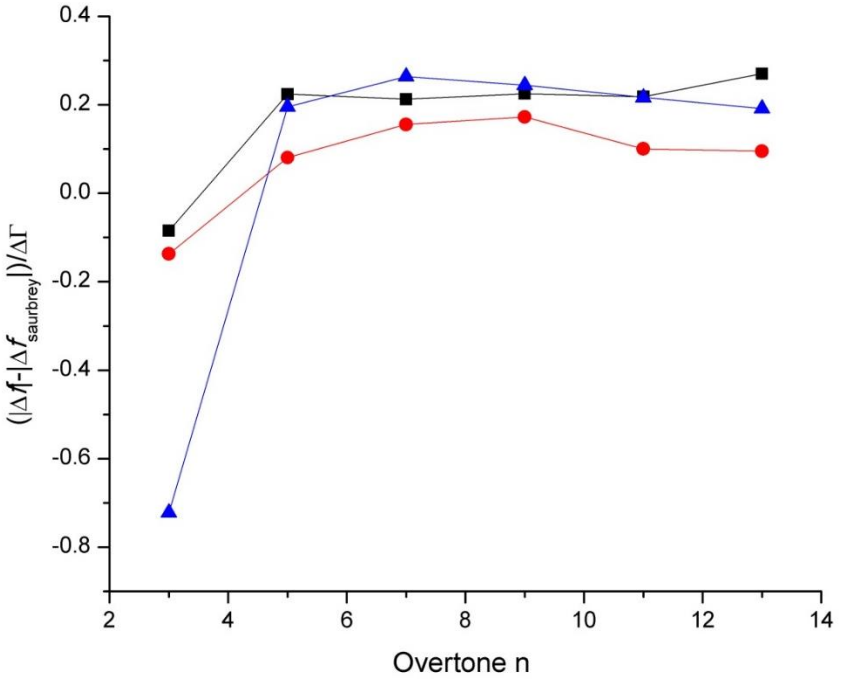

Figure 20. Comparison of (|Δf|-|Δf_sauerbrey |/ΔΓ) beetween the experimental results in red and blue; and in black a hypothetical case with a 150 nm film with a density of 965 kg/m3 using the kelvin voigt model.

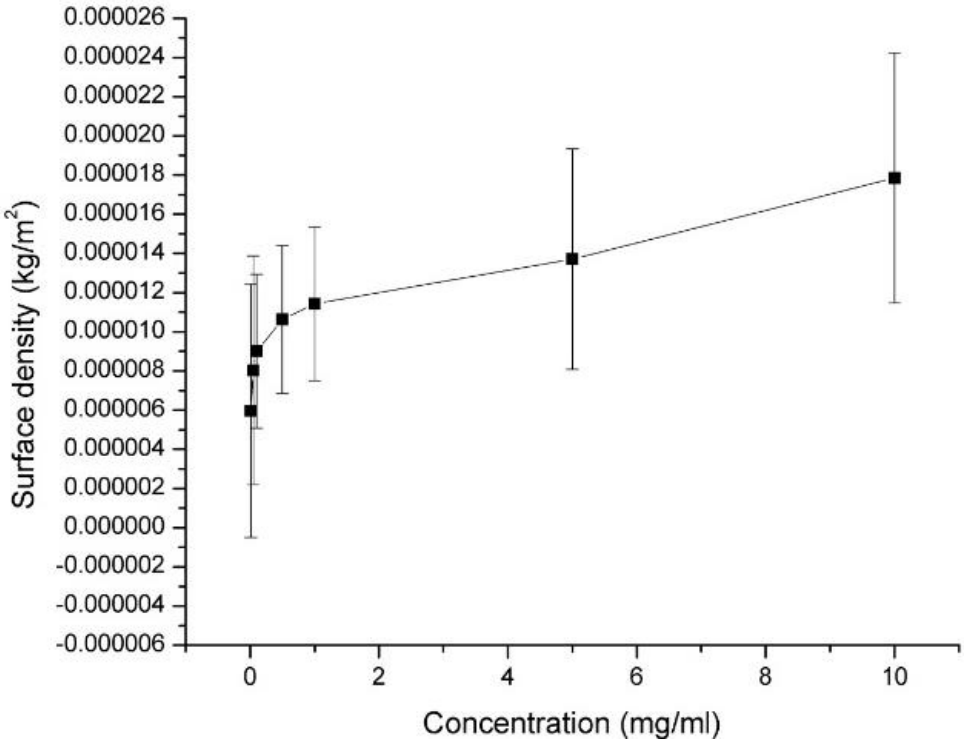

Figure 21. Mean surface density for PEI films using a pH 7. The mean and the confidence intervals for 3 experiments are shown.

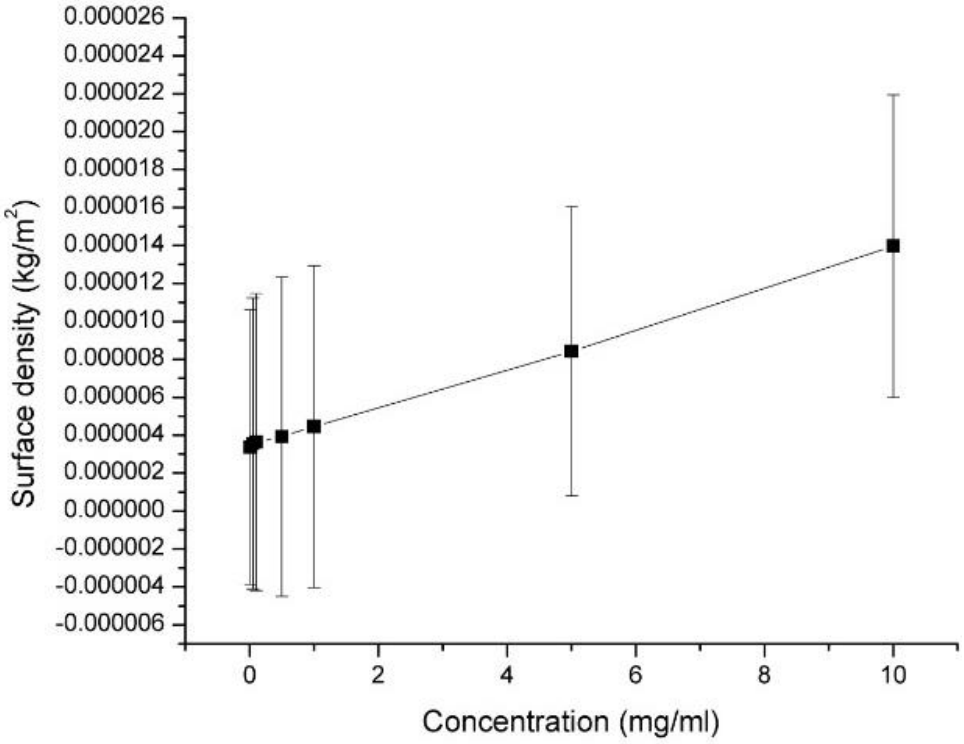

Figure 22. *Mean surface density for PEI films using a pH 12.* The mean and the confidence intervals for 3 experiments are shown.

The viscoelastic properties of PDMS have been documented in the literature owing to its widespread applications, characterized by user-friendliness, advantageous mechanical qualities (notable elasticity), biocompatibility, and transparency. In a study by V. Placet and P. Delobelle the dynamic mechanical characterisation of polydimethylsiloxane (PDMS) over a wide frequency range ($10^{-2} < f < 10^5$ Hz) and lengthy room temperature aging durations (4 h < tv < ~60 000 h) has been presented. Three samples with varying curing conditions were investigated using three different techniques: dynamic mechanical analysis (DMA) at different temperatures, nano-indentation, and scanning micro-deformation microscopy (SMM). Although the three methods operate at different frequencies and at different scales (micro and macro), as the frequency ($0.01 < f < 10^5$ Hz) increases, E′ and E″ rise from 2 to 7.5 MPa and 0.02 to 1.6 MPa, respectively. It is noteworthy that the results of SMM (f ~ 3 and 4.5 kHz) and nano-indentation (quasi-static and dynamic (f = 45 Hz)) precisely match the master curves derived from the DMA procedure (0.01–80 Hz). In another study, Shinji Deguchi and colleagues investigated the viscoelastic properties of four different types of PDMS; we are

focusing on the results for Sylgard-184 because we have also analyzed it. Both this study and the previous one prepared PDMS according to the manufacturer's instructions, which calls for a 10:1 ratio of polymer base to curing agent. It is important to mention as for some applications the quantity of curing agent is generally reduced to provide a softer cured PDMS. For our experiments we used half the quantity of the curing agent and the polymer base was diluted according to the protocol proposed by M. Bračič et al. In order to characterize the viscoelastic properties, Shinji Deguchi et al. Used dynamic mechanical spectroscopy at 1 Hz to determine the loss tangent, or tanδ. This quantifies the relative contribution of elasticity and viscosity and is the ratio of the loss modulus E″ to the storage modulus E′. Regardless of the PDMS type, results demonstrate that the value of tanδ, which should be zero for ideal elastic materials, is less than 0.1. This tendency persisted irrespective of the temperature examined. Consequently, PDMS has significant elasticity with minimal energy dissipation. It is important to note that for frequencies over 10 Hz, Sylgard-184 demonstrated a loss tangent greater than 0.1. At 25° E′ is less than 2MPa and E'' is around 0.05 MPa.

D. Armani et al. Performed an experimental investigation to ascertain the mechanical properties of PDMS, encompassing the Young's modulus and adhesion energy. Young's modulus varies from 8.7 x 10^5 Pa to 3.6 x 10^5 Pa, depending on polymer base to curing agent ratios of 1:5 to 1:15. Our tests were conducted between 5 and 65 MHz. The values for G" and G' range from 5 to 15 MPa and 1 to 6 MPa, respectively. It is evident that the values fluctuate as the frequency increases, and that the viscous modulus is more significant than the elastic modulus, in contrast to the findings of the literature. This may result from modifications in the mixing ratio, the dilution of the polymer base with toluene, the curing time, and the thickness of the films employed. Despite this our results are in the same magnitude order as the ones reported in literature. A. Strony & W.W Gerberich determined the elastic modulus of PDMS films with thicknesses of 2.0 and 7 micrometers was measured at 90 MPa and 10 MPa, respectively; thinner films have greater modulus values due to substrate effects. The indentation values fell within the range obtained from dynamic mechanical analysis. A three-element

model comprising a spring in series with a Kelvin-Voigt element demonstrated an excellent fit. The model permitted the determination of shear and elastic modulus values from load relaxation and creep testing. We also used a Kelvin-Voigt model for QCM-D data analysis as It demostrated a good fit.

Typically, layer-by-layer assembly involves the alternating interaction of a polyanion and a polycation to create polyelectrolyte multilayers on different kind of surfaces, especially for sensing or biomedical applications. Adsorption in these systems is often facilitated by electrostatic interactions with a charged substrate. Adsorption leads to charge overcompensation, hence promoting the subsequent adsorption of an oppositely charged polyelectrolyte. This user-friendly approach enables straightforward control over the surface charge and film thickness. Despite being uncommon, a polyelectrolyte multilayer film consisting of a single polyelectrolyte can be produced. For example in a study by Tao He & Vicent Chan, covalent LBL deposition was used to create a stable polyelectrolyte multilayer film consisting entirely of polyethyleneimine (PEI). The initial step involved the validation of the specific PEI accumulation during covalent LBL assembly using atomic force microscopy and UV-Vis absorption spectroscopy. In our case,we employed the QCM-D to monitor the build-up of PEI layers and the changes in film thickness due to changes in PEI solution concentration and pH. In our results we see that with increasing concentration, there is a bigger disminution in the frequency which is directly related with an increase in film thinckness or surface density. Also we see differences with pH an increase surface density at pH 7. PEI has many uses, including as a vector for nonviral gene delivery due to its high transfection efficiency and pH responsiveness. Caleb E. Gallops et al. conducted atomistic molecular dynamics simulations of a linear PEI chain for nine protonation states and different NaCl concentrations in a study to investigate the relationship between linear PEI structure, pH, and salt content. They found that when PEI goes from being unprotonated to fully protonated, it keeps expanding; protonation decreases with the augmentation of pH. Branched PEI exhibits elevated concentrations of primary, secondary, and tertiary amines, with only 15–20% being

protonated at physiological pH. This may explain the reduction in PEI surface density or PEI -PEI interaction.

7.4Conclusion

We employed QCM-D to analyze polymer films, focusing on the viscoelasticity of PDMS and the adsorption of PEI. QCM-D is an excellent instrument for this application, as it facilitates the utilization of thin films. We select these polymers due to their diverse uses in biomedicine and biotechnology. The applications of PDMS encompass cellular development, implants, and catheters, highlighting the necessity of adjusting its viscoelastic properties suitably. Our thin films demonstrate significantly greater viscous moduli compared to elastic moduli, contrary to the prevailing literature. PEI has various applications, including DNA transport and functioning as an antibacterial agent. Regulating PEI deposition and, subsequently, film thickness is essential for the application of PEI films, particularly in medical instruments, to inhibit biofilm formation. We found that pH is critical in film deposition, as PEI is responsive to pH variations.

7.5 References

1. Liu, Gehui. (2022). *Quartz crystal microbalance with dissipation monitoring applications in polymer thin films analysis* (dissertation). *Quartz Crystal Microbalance with Dissipation Monitoring Applications in Polymer Thin Films Analysis*. Virginia Tech.
2. Biolin Scientific . (n.d.). Polymer studies by QCM-D.
3. Edvardsson, M. (2019, October). *Using QCM-D to analyze thin polymer films*. Biolin Scientific. https://www.biolinscientific.com/blog/how-to-characterize-polymer-based-systems-with-qcm-d
4. Easley, A. D., Ma, T., Eneh, C. I., Yun, J., Thakur, R. M., & Lutkenhaus, J. L. (2021). A practical guide to quartz crystal microbalance with dissipation monitoring of thin polymer films. *Journal of Polymer Science*, *60*(7), 1090–1107. https://doi.org/10.1002/pol.20210324
5. Baldelli, A., Esmeryan, K. D., & Popovicheva, O. (2021). Turning a negative into a positive: Trends, guidelines and challenges of developing multifunctional non-wettable coatings based on industrial soot wastes. *Fuel*, *301*, 121068. https://doi.org/10.1016/j.fuel.2021.121068
6. Bračič, M., Mohan, T., Kargl, R., Griesser, T., Hribernik, S., Köstler, S., Stana-Kleinschek, K., & Fras-Zemljič, L. (2014). Preparation of PDMS ultrathin films and patterned surface modification with cellulose. *RSC Adv.*, *4*(23), 11955–11961. https://doi.org/10.1039/c3ra47380e
7. Miranda, I., Souza, A., Sousa, P., Ribeiro, J., Castanheira, E. M., Lima, R., & Minas, G. (2021). Properties and applications of PDMS for Biomedical Engineering: A Review. *Journal of Functional Biomaterials*, *13*(1), 2. https://doi.org/10.3390/jfb13010002
8. Bračič, M., Mohan, T., Griesser, T., Stana-Kleinschek, K., Strnad, S., & Fras-Zemljič, L. (2017). One-step noncovalent surface functionalization of PDMS with chitosan-based Bioparticles and their protein-repellent properties. *Advanced Materials Interfaces*, *4*(21). https://doi.org/10.1002/admi.201700416
9. Cao, Y., Fu, M., Fan, S., Gao, C., Ma, Z., & Hou, D. (2024). Hydrophobic MOF/PDMS-based QCM sensors for vocs identification and quantitative detection in high-humidity environments. *ACS Applied Materials & Interfaces*, *16*(6), 7721–7731. https://doi.org/10.1021/acsami.3c16228
10. Saidin, S., Jumat, M. A., Mohd Amin, N. A., & Saleh Al-Hammadi, A. S. (2021). Organic and inorganic antibacterial approaches in combating bacterial infection for biomedical application. *Materials Science and Engineering: C*, *118*, 111382. https://doi.org/10.1016/j.msec.2020.111382
11. Samal, S., Mohanty, S., & Nayak, S. K. (2019). *Superhydrophobic polymer coatings: Fundamentals, design, fabrication, and applications*. Elsevier.
12. Aulin, C., Varga, I., Claesson, P. M., Wågberg, L., & Lindström, T. (2008). Buildup of polyelectrolyte multilayers of polyethyleneimine and microfibrillated cellulose studied by in situ dual-polarization interferometry and quartz crystal microbalance with dissipation. *Langmuir*, *24*(6), 2509–2518. https://doi.org/10.1021/la7032884
13. Findenig, G., Kargl, R., Stana-Kleinschek, K., & Ribitsch, V. (2013). Interaction and structure in Polyelectrolyte/Clay Multilayers: A QCM-D study. *Langmuir*, *29*(27), 8544–8553. https://doi.org/10.1021/la400880a
14. Saffari, Z., Sepahi, M., Ahangari-Cohan, R., Khoobi, M., Hamidi-Fard, M., Ghavidel, A., Aghasadeghi, M. R., & Norouzian, D. (2023). A quartz crystal microbalance biosensor based on polyethylenimine-modified gold electrode to

detect hepatitis B Biomarker. *Analytical Biochemistry*, *661*, 114981. https://doi.org/10.1016/j.ab.2022.114981
15. Rawle, R. J., Johal, M. S., & Selassie, C. R. (2007). A real-time QCM-D approach to monitoring mammalian DNA damage using DNA adsorbed to a polyelectrolyte surface. *Biomacromolecules*, *9*(1), 9–12. https://doi.org/10.1021/bm701062f.
16. Placet, V., & Delobelle, P. (2015a). Mechanical properties of bulk polydimethylsiloxane for microfluidics over a large range of frequencies and aging times. *Journal of Micromechanics and Microengineering*, *25*(3), 035009. https://doi.org/10.1088/0960-1317/25/3/035009
17. Deguchi, S., Hotta, J., Yokoyama, S., & Matsui, T. S. (2015a). Viscoelastic and optical properties of four different PDMS polymers. *Journal of Micromechanics and Microengineering*, *25*(9), 097002. https://doi.org/10.1088/0960-1317/25/9/097002
18. D. Armani, C. Liu and N. Aluru, "Re-configurable fluid circuits by PDMS elastomer micromachining," Technical Digest. IEEE International MEMS 99 Conference. Twelfth IEEE International Conference on Micro Electro Mechanical Systems (Cat. No.99CH36291), Orlando, FL, USA, 1999, pp. 222-227, doi: 10.1109/MEMSYS.1999.746817.
19. Stroiny, A., Gerberich, W.W. Experimental Analysis of Viscoelastic Behavior in Nanoindentation. *MRS Online Proceedings Library* **522**, 159–164 (1998). https://doi.org/10.1557/PROC-522-159
20. Ferreyra, N. F., Bollo, S., & Rivas, G. A. (2010). Self-assembled multilayers of polyethylenimine, DNA and gold nanoparticles. A study of electron transfer reaction. *Journal of Electroanalytical Chemistry*, *638*(2), 262–268. https://doi.org/10.1016/j.jelechem.2009.11.009
21. He, T., & Chan, V. (2010). Covalent layer-by-layer assembly of polyethyleneimine multilayer for antibacterial applications. *Journal of Biomedical Materials Research Part A*, *95A*(2), 454–464. https://doi.org/10.1002/jbm.a.32872
22.
23. He, T., & Chan, V. (2010a). Covalent layer-by-layer assembly of polyethyleneimine multilayer for antibacterial applications. *Journal of Biomedical Materials Research Part A*, *95A*(2), 454–464. https://doi.org/10.1002/jbm.a.32872
24. Benoit, D.S.W. & Gray, W. & Murthy, N. & Li, H. & Duvall, C.L.. (2017). 4.26 pH-Responsive Polymers for the Intracellular Delivery of Biomolecular Drugs. 10.1016/B978-0-08-100691-7.00019-7.

Appendix 2

Articles published

- Jonguitud-Flores, S., Yáñez-Soto, B., Pérez, E., & Sánchez-Balderas, G. (2024). Wetting transitions in adhesive surfaces of polystyrene: The petal effect. *Journal of Colloid and Interface Science*, *674*, 178–185.

- Pardi, B., Ahmed, S. T., Flores, Jonguitud-Flores, S., W., Friedt, J.-M., Mears, L. L., Soto, B. Y., & Eguiluz, R. C. (2024). PyQCM-BraTaDio: A tool for visualization, data mining, and modelling of quartz crystal microbalance with dissipation data. *Journal of Open Source Software*, *9*(99), 6831.

- Vélez-Cordero, J. R., Jonguitud Flores, S., & Yáñez Soto, B. (2024). Finite element simulations of quartz crystal microbalances (QCM): From Sauerbrey to fractional viscoelasticity under water. *Physica Scripta*, *99*(11), 115963.